

**Semiconductor Laser Noise and Linewidth Reduction and
Rayleigh Scattering in Optical Fibers**

Thesis by

Shu-Wu Wu

In Partial Fulfillment of the Requirements

for the Degree of

Doctor of Philosophy

California Institute of Technology

Pasadena, California

1992

(Submitted May 28, 1992)

To My Wife, Virginia

Acknowledgements

I would like to express my deepest gratitude to Professor Amnon Yariv, my advisor, who not only educated me in quantum electronics but literally guided me into applied science. His dynamic vision and keen physical insight continually provided invaluable and thought provoking guidance. It has truly been both a privilege and rewarding experience to work in the creative atmosphere of his research group.

I am grateful to my wife, Virginia, for her understanding and constant support throughout the Caltech years.

Special thanks to Dr. Sidney Kan who taught me device processing and collaborated with me on a number of projects which are not presented in this thesis.

I would like to express my appreciation to Dr. Yasuo Tomita who patiently worked with me during my first year with the group. I have significantly benefited from his excellent technical knowledge and experimental skills.

I am greatly indebted to Professor T. R. Chen who provided wafers and invaluable tips on the processing of multiple section stripe lasers.

Special thanks to Dr. Steve Sanders, Mr. Bill Marshall, and Dr. Yaakov Shevy for laboratory assistance and fruitful discussions. Thanks are also extended to Dr. Howard Chen, Mr. Bin Zhao, Dr. Giora Griffel, Mr. Ilan Grave, Dr. Victor Leyva, Dr. Aharon Agranat, and Dr. Koichi Sanyano for their many helpful discussions and assistance.

I would like to thank Mrs. Jana Mercado and Mr. Ali Gaffari for the help I

received during my stay with the group.

Finally, the financial support of the California Institute of Technology is greatly appreciated.

Abstract

This thesis is a theoretical and experimental investigation of monolithic linewidth reduction in multiple section distributed-feedback (DFB) lasers and of phase-to-intensity conversion noise due to Rayleigh scattering in optical fiber links. In the first part, the physics of semiconductor laser dynamics and noise is reviewed. A Van der Pol noise analysis of laser amplitude and phase fluctuations is conducted. Linewidth reduction in lasers with intra-cavity dispersive medium is analyzed. The semiconductor laser subjected to an external optical feedback is studied by treating the feedback as a part of facet complex reflectivity.

In the second part, a theoretical study of three section semiconductor DFB lasers is presented. The result shows that under proper pumping and biasing conditions one section lases while the other provide the necessary dispersive optical feedback for noise suppression and, hence, linewidth reduction. The benefits of having such optical feedback on modulation responses is also demonstrated.

An experimental study of three section semiconductor DFB lasers is presented in the third part. Processing and standard testing procedures of the multiple section DFB laser is described. Subsequently the scanning Fabry-Perot, optical spectrum analyzer, and the delayed-self-heterodyne method are used for the measurements. The experimental results demonstrate a moderate reduction in laser linewidth.

In the fourth part, a complete statistical theory, including the effect of random fiber index inhomogeneities, of conversion of fundamental phase fluctuation at

semiconductor laser output to intensity noise in long haul optical fiber links due to Rayleigh scattering is developed. Three generic cases are considered.

In part five, a detailed experimental study of Rayleigh induced intensity fluctuations is presented. Comparison between the theoretically predicted and experimentally measured values shows very good agreement.

The impact of Rayleigh scattering on fiber links with periodic optical amplification is considered. The result shows linear accumulation of intensity noise due to Rayleigh scattering. To prevent a quadratic accumulation of the Rayleigh scattering induced intensity noise, optical isolators in very long haul fiber links are required. A reduction scheme of phase-to-intensity conversion noise by phase modulation is subsequently studied.

Table of Contents

Acknowledgements	iii
Abstract	v
Table of Contents	vii
List of Figures	xi
1 An Introduction	1
1.1 Fiber-Optic Telecommunication Systems	1
1.2 Outline of the Thesis	5
1.3 References	8
2 Semiconductor Lasers Noise and Linewidth Reduction	10
2.1 Semiconductor Lasers: Double Heterostructure and Quantum Well Lasers	10
2.2 Spontaneous Emission	12
2.3 Semiclassical Theory of Semiconductor Laser Noise	16

2.4	Laser Spectral Properties	21
2.5	Intra-Cavity Dispersive Medium	24
2.6	Semiconductor Laser Exposed to External Optical Feedbacks	26
2.7	References	31
3	Theory of Monolithic Semiconductor Laser Linewidth Reduction	34
3.1	A Simplified Model	35
3.2	Distributed-Feedback Lasers	40
3.3	Multiple Section Distributed-Feedback Lasers	42
3.4	References	48
4	Experimental Study of Multiple Section Distributed-Feedback Semiconductor Lasers	49
4.1	DFB Laser Structure	49
4.2	Processing of Multiple Section DFB Lasers	50
4.3	Experiment and Results	52
4.4	Discussions	59
4.5	References	61
5	Rayleigh Scattering Induced Phase-to-Intensity Noises in Optical Fibers	62
5.1	An Introduction	62

5.2	Statistics of Semiconductor Laser Noise and Index Fluctuations in Optical Fibers	64
5.3	Theory of Phase-to-Intensity Conversion Noise due to Rayleigh Scattering in Optical Fibers	68
5.4	References	75
6	Experimental Study of Rayleigh Scattering Induced Intensity Noise in Optical Fibers	77
6.1	An Introduction	77
6.2	Measurement of the Coherence Time	78
6.3	Rayleigh Scattering	80
6.4	Summary	90
6.5	References	91
7	Rayleigh Scattering in Fiber Links with Periodic Optical Amplification and a Proposed Noise Reduction Scheme	92
7.1	Fiber Links with Periodic Optical Amplification	92
7.2	Reduction of Rayleigh Scattering Induced Noise by Pre-Phase Modulation of the Optical Field	97
7.3	Comments on Future Work Related to Rayleigh Scattering in Optical Fibers	105
7.4	References	107

A Wick's Theorem	109
B Delayed-Self-Homodyne Measurement Technique	112

List of Figures

2.1	Laser power versus pumping	14
2.2	Phasor diagram of laser field	15
2.3	A simple semiconductor laser	18
2.4	A semiconductor laser exposed to external feedback	27
3.1	A two section semiconductor laser	36
3.2	A three section DFB laser structure	43
4.1	Experimental setup for laser linewidth measurements	54
4.2	Measured optical spectrum of a DFB laser	56
4.3	Observation of laser linewidth reduction (#1)	57
4.4	Observation of laser linewidth reduction (#2)	58
5.1	Double Rayleigh scattering in optical fibers	69
5.2	Redirected Rayleigh scattering in optical fibers	69
5.3	Rayleigh backscattering in optical fibers	70
6.1	Delayed-self-homodyne detection	80

6.2	Experimental setup and photocurrent spectrum for double Rayleigh scattering in optical fibers	84
6.3	Experimental setup and photocurrent spectrum for redirected Rayleigh scattering in optical fibers	87
6.4	Measurement of RF signal level	88
6.5	Experimental setup and photocurrent spectrum for Rayleigh backscattering in optical fibers	89
7.1	Fiber links with periodic optical amplification	93
7.2	Noise reduction by optical phase modulation	99
7.3	Noise reduction factor	104

Chapter 1

An Introduction

1.1 Fiber-Optic Telecommunication Systems

One of the most important factors responsible for successful large scale applications of fiber-optic telecommunications [1] today and in the near future is that silica glass fiber has low optical propagation losses. After 30 years of continuous improvements in the manufacturing processes, today we have optical fibers with very low losses $\sim 0.2\text{dB}/\text{km}$ at wavelengths near $1.55\mu\text{m}$ [2]. The $1.55\mu\text{m}$ region is now favored for long-distance optical communications. Furthermore, the silica glass fiber offers a large region of low optical loss near $1.55\mu\text{m}$ which can yield up to a 10THz optical transmission bandwidth [2]. As a result, there is a substantial effort being expended in the search for tunable semiconductor lasers and developing multiplexing systems for the interconnects. The single-mode fiber has another useful feature in that it has zero group velocity dispersion at $\sim 1.3\mu\text{m}$ wavelength [3]. Since no modal dispersion exists

(only one mode allowed in a single-mode fiber), it is dispersion free at $1.3\mu m$ where the loss is approximately $0.4dB/km$ [2]. Consequently, for the amplitude modulation (AM) communication systems over intermediate range distances, $1.3\mu m$ is the ideal working wavelength. There are now fibers whose zero dispersion λ have been shifted to $1.55\mu m$ [3].

Another important factor responsible for the optical fiber as a favored transmission medium is that it offers high data transmission rates over long distance which is unparalleled in its electronic counterpart [2,4]. The high data transmission rate is crucial for image transmission, remote data acquisition, and the emerging technology called "Multi-media communications." Recent developments of optical amplification along fiber links [5,6,7] have made optical fiber a viable medium for information transmission over very long distances ($> 1000km$). Major effort has been devoted to develop and study the Erbium-doped fiber that can provide necessary amplification, which periodically boosts the optical signal back up to its original level, so that conventional electronic repeaters are not required.

Of course, the success of silica glass fiber itself does not completely account for the prominence of fiber-optic telecommunication technology. Advancement in the field of semiconductor lasers at the fundamental research level, as well as in commercial applications, have contributed, in large part, to the successes. The InGaAsP/InP material system is now widely used as the semiconductor laser sources for fiber-optic telecommunications because it provides coherent light at the required wavelengths (near $1.55\mu m$ and $1.3\mu m$) [4]. In contrast to the GaAs/AlGaAs system, it has the

advantage of variable lasing wavelength by simply changing the fractional composition of InGaAsP. The introduction of ultra-low threshold quantum well lasers [8] and recent advances in high frequency modulation and passive mode-locking has made the semiconductor laser the single most important laser in today's technology.

Advancement of fiber-optic telecommunication technology at both the research and commercial levels has generated a great deal of interest in searching for narrow linewidth semiconductor laser sources and in studying and reducing the phase-to-intensity fluctuations which arise from Rayleigh scattering in fiber links. The purpose of this work is to address the two issues both theoretically and experimentally.

Commercial semiconductor lasers typically have linewidths of 10 to 20MHz because of short laser cavity length (typically $300\mu m$). Traditionally the semiconductor laser linewidth can be drastically reduced by introducing external optical feedback [9] which effectively converts it into an external cavity laser. In the process the semiconductor laser loses one of its greatest advantages, that of being a micro-device that can be compactly integrated with the electronics. Therefore, substantial effort has been put forth to achieve a compact semiconductor laser with a narrow linewidth. D. A. Ackerman, et al. at AT&T Bell Laboratories, Murray Hill, NJ, successfully developed compact hybrid resonant optical reflector lasers with a linewidth as low as 7.1kHz [10], but with a disadvantage that it is not monolithic. Ohtsu et al. at Tokyo Institute of Technology, Japan, achieved linewidth as narrow as 250Hz in a DFB InGaAsP laser using the negative electronic feedback (NEF) [11] but, again, considerable complex external feedback configuration was required. The more aggressive goal is to obtain

a monolithic narrow linewidth semiconductor laser. Various groups in Japan have used multiple section distributed-feedback (DFB) lasers with inhomogeneous pumping and/or phase shifting to achieve significant reductions in laser linewidth [12,13]. M. Okai, et al. at Hitachi Central Research Laboratory, Tokyo, used a corrugation-pitch-modulated DFB laser to achieve a 170kHz linewidth [14]. However, thus far all monolithic semiconductor lasers have failed to achieve the drastic linewidth reduction using external feedbacks. In this thesis a reduction scheme employing three section DFB lasers in a completely different perspective is presented. In lieu of pumping all sections positively, it was proposed to reverse bias the center section which effectively reduces the interaction between end sections to the weak interaction regime. It was proposed to pump one end section above its threshold and to pump the second end section close but below its threshold. The theoretical study indicated that in such pumping condition, the second end section provides optical feedback to the first end section that has similar characteristics of an external optical feedback from a Fabry-Perot etalon. This offers the possibility of a similar drastic reduction as in an external feedback scheme. The experimental study has achieved a moderate reduction in laser linewidth under proposed pumping conditions.

A theoretical study of Rayleigh scattering of single-mode fibers was presented in 1980 [15,16]. Since then a number of studies have been conducted on Rayleigh scattering in fibers and the related issue of phase-to-intensity conversion noise [17,18]. However, a full statistical analysis of the problem has not been developed. In the second part of this thesis, a statistical theory of the mixing of the Rayleigh scattered and

the direct transmitted light and the resulting intensity noise is presented. The theory includes a complete description of the statistical nature of the laser phase fluctuation and index inhomogeneities in optical fibers. Then a detailed experimental study was conducted under various generic scenarios with varying fiber lengths. A comparison with the theoretical predictions is subsequently presented. The results demonstrate extremely good agreement between the theory and the actual measurements. The impact of Rayleigh scattering in the fiber links with periodic optical amplification is also presented. Finally, a noise reduction scheme by phase modulation at high frequency is studied.

1.2 Outline of the Thesis

In Chapter 2, semiconductor laser dynamics and noise is reviewed. The Langevin-oscillator equation governing laser amplitude and phase fluctuations is introduced. Its solution is then used to derive various spectral properties of semiconductor lasers. Semiconductor lasers exposed to external optical feedback are considered and linewidth reduction in lasers (any laser) with intra-cavity dispersive medium is analyzed in the context of self-quenching effect by phase-to-amplitude coupling.

In Chapter 3, three section semiconductor DFB lasers are proposed as a possible mechanism to achieve drastic linewidth reduction. Theoretical analysis shows that under proper pumping and biasing conditions one section lases while the other provide the necessary dispersive optical feedback for noise suppression and, hence, linewidth

reduction. The analysis also demonstrates the benefits of having such optical feedback on the modulation response.

An experimental study of three section semiconductor DFB lasers is described in Chapter 4. The complex fabrication and processing procedure of the multiple section DFB laser is described. The linewidth measurement techniques involving scanning Fabry-Perot, optical spectrum analyzer, and delayed-self-heterodyne method are subsequently used. The experimental results and a few comments are presented.

A complete statistical theory of conversion of fundamental phase fluctuation at semiconductor laser output to intensity noise in long haul optical fiber links due to Rayleigh scattering is described in Chapter 5. Three generic cases are considered and the results are simple expressions of spectral density functions for photocurrent at detection as well as the laser power that is Rayleigh backscattered.

A detailed experimental study of Rayleigh induced intensity fluctuation is presented in Chapter 6. The laser coherence time was measured by the delayed-self-homodyne method and the only material parameter in the theory was determined by using the experimental relative intensity noise data. Comparison between the theoretical predictions and measurement data is carried out and very good agreement is shown.

Finally, in Chapter 7, the impact of Rayleigh scattering on fiber links with periodic optical amplification is considered. A comparison of the Rayleigh scattering induced intensity fluctuations and noise due to beating between signal and amplifier spontaneous emission is conducted. The significance of the presence of optical isola-

tors in very long haul fiber links, to prevent the quadratic accumulation of Rayleigh scattering induced noise, is demonstrated. A reduction scheme of phase-to-intensity conversion noise by phase modulation of optical carrier at high frequencies is proposed and analyzed.

1.3 References

- [1] D. Botez, G. J. Herskowitz, *Proc. IEEE*, **68**, 1980.
- [2] T. Miya, Y. Terunuma, T. Hosaka, and T. Miyashita, *Electron. Lett.*, **15**, 106(1979).
- [3] A. Yariv, *Optical Electronics*, 4th ed. (Holt, Rinehart and Winston, Philadelphia, 1991), and references therein.
- [4] Y. Suematsu, *Proc. IEEE*, **71**, 692(1983).
- [5] J. C. Simon, *J. Opt. Commun.*, **4**, 51(1983).
- [6] R. J. Mears, L. Reekie, I. M. Jauncey, and D. N. Payne, *Electron. Lett.*, **23**, 1026(1987).
- [7] K. Hagimoto, et al., *Proceedings of the Optical Fiber Conference*, Houston, TX, postdeadline paper PD15, 1989.
- [8] P. Derry, et al., *Appl. Phys. Lett.*, **50**, 1773(1987).
- [9] P. H. Laurent, A. Clairon, and C. H. Breaut, *IEEE J. Quant. Elec.*, **25**, 1131(1989).
- [10] D. A. Ackerman, M. I. Dahbura, Y. Shani, C. H. Henry, R. C. Kistler, R. F. Kazarinov, and C. Y. Kuo, *Appl. Phys. Lett.*, **58**, 449(1991).
- [11] M. Ohtsu et al., presented at the *IEEE Lasers and Electro-Optics Society Conference*, San Jose, California, 1991, Paper SADL4.1.

- [12] Y. Kotaki, et al., *Electron. Lett.*, **25**, 990(1989).
- [13] M. Kitamura, et al., *IEEE Photon. Tech. Lett.*, **2**, 310(1990).
- [14] M. Okai, T. Tsuchiya, K. Uomi, N. Chinone, and T. Harada, *IEEE Photon. Tech. Lett.*, **2**, 529(1990).
- [15] E. Brinkmeyer, *J. Opt. Soc. Am.*, **70**, 1010(1980).
- [16] E. Brinkmeyer, *Electron. Lett.*, **16**, 329(1980).
- [17] A. F. Judy, presented at the *European Conference on Optical Communication*, Gteborg, Sweden, 1989, paper TuP-11.
- [18] J. Mark, Ph.D. thesis, Electromagnetics Institute, Technical University of Denmark, Lyngby, Denmark.

Chapter 2

Semiconductor Lasers Noise and Linewidth Reduction

2.1 Semiconductor Lasers: Double Heterostructure and Quantum Well Lasers

The semiconductor diode laser was invented in 1961 [1,2,3]. Since then it has become, possibly, the most important laser in terms of technological importance and mass commercial applications. The semiconductor laser is characterized by its small physical size (a micro-device) and monolithic integrability with optoelectronics, its high frequency modulation for high speed data communications, and, perhaps most importantly, its compatibility with optical fibers.

The stimulated emission from semiconductors was first observed from a *pn* [1,2,

3] junction. However, semiconductor lasers using the double heterostructure [4,5,6] have been shown to be far superior. Typically a double heterostructure consists of an intrinsic (undoped) layer of $0.1\mu\text{m}$ thickness sandwiched between two heavily oppositely doped layers which have higher bandgap energies than the middle layer. The optical gain is provided by injecting current into the middle layer where electrons recombine with the holes. The difference in bandgap energies effectively traps the electrons in the middle layer (called active region) so that nearly all the electrons participate in transition to the valence band. An additional advantage of the double heterostructure is that the active layer has a slightly higher index of refraction than the cladding layers so they effectively form an optical waveguide [7,8].

The two most important material systems for semiconductor laser applications are $GaAs/Ga_{1-x}Al_xAs$ and $In_xGa_{1-x}As_{1-y}P_y/InP$. Especially lasers based on the second material system has $In_xGa_{1-x}As_{1-y}P_y$ as the active region whose bandgap energy can be tuned to emit in $1.1\mu\text{m} < \lambda < 1.6\mu\text{m}$ by simply changing the fractional compositions x and y . As a result, $In_xGa_{1-x}As_{1-y}P_y/InP$ based lasers are widely utilized as coherent light sources for fiber-optic telecommunications.

The quantum size effect takes place when the active layer is very thin ($\leq 100 \text{ \AA}$). This results in a new class of semiconductor lasers designated as quantum well (QW) lasers [9,10]. Because the active region is reduced in thickness by a factor of 10, the threshold current density is reduced approximately by the same factor. Consequently, a class of ultra-low threshold semiconductor lasers [11] results. QW lasers offer numerous advantages over conventional semiconductor lasers and quantum bandgap

engineering opens up a new field associated with quantum effects [12,13,14].

2.2 Spontaneous Emission

In this section we consider the essential ingredients of laser action. A typical laser requires a cavity formed by two mirrors (of course theoretically a mirrorless oscillator is possible and is not relevant here) and a gain medium within the cavity. At room temperature, without a pumping mechanism, virtually all the electrons are in the groundstate energy level, hence, there is an insufficient population of electrons in excited energy levels to allow for laser action to occur. In semiconductor, the laser transition is between the conduction and valence bands. Because of the time-reversal invariance in quantum physics, the stimulated transition from the groundstate to the excited state (loss) is at the same rate as that from the excited state to the ground state (gain). Consequently, net gain results only when there are more electrons in the excited energy level than that in the groundstate energy level, a configuration called negative temperature state. The threshold conditions for a laser to begin lasing is twofold:

1. The gain equals the total optical losses (including medium, mirrors, etc.) in a round trip.
2. The round trip phase delay equals a multiple of 2π .

Under ordinary pumping conditions, the number of quantum modes that undergoes spontaneous emission in the laser cavity is

$$p = \frac{8\pi\nu^2\Delta\nu n^3V}{c^3} \quad (2.1)$$

where ν is the laser frequency, $\Delta\nu$ is the linewidth of the excited energy level, specifically, only frequencies within $\sim \Delta\nu$ of the line center are effective in inducing a transition (in semiconductor laser, $\Delta\nu$ is the bandwidth of the gain), n is the index of refraction of the laser medium, V is the laser cavity volume, and c is the speed of light in vacuum. Below the threshold, the stimulated transition rate is zero and the total spontaneous emission power is divided, roughly evenly, among all p possible modes.

When the pumping is increased from below to above the threshold, one mode is singled out because it satisfies the round trip phase condition and the round trip gain is greater than the total losses. Electric field fluctuation (due to spontaneous emission) grows after every round trip (because of the net gain) and, therefore, a non-zero radiation field is established. Consequently, the stimulated transition rate for the mode becomes nonzero and further accelerates the build-up of the radiation field. This chain reaction results in continual increase of the radiation field strength until the gain is saturated and equals the total losses in a round trip and, hence, steady state oscillation results. Further increase in the pumping rate results in virtually all of the increased radiation power feeding into the lasing mode. In contrast, below threshold, the increased radiation power is divided, more or less equally, among all

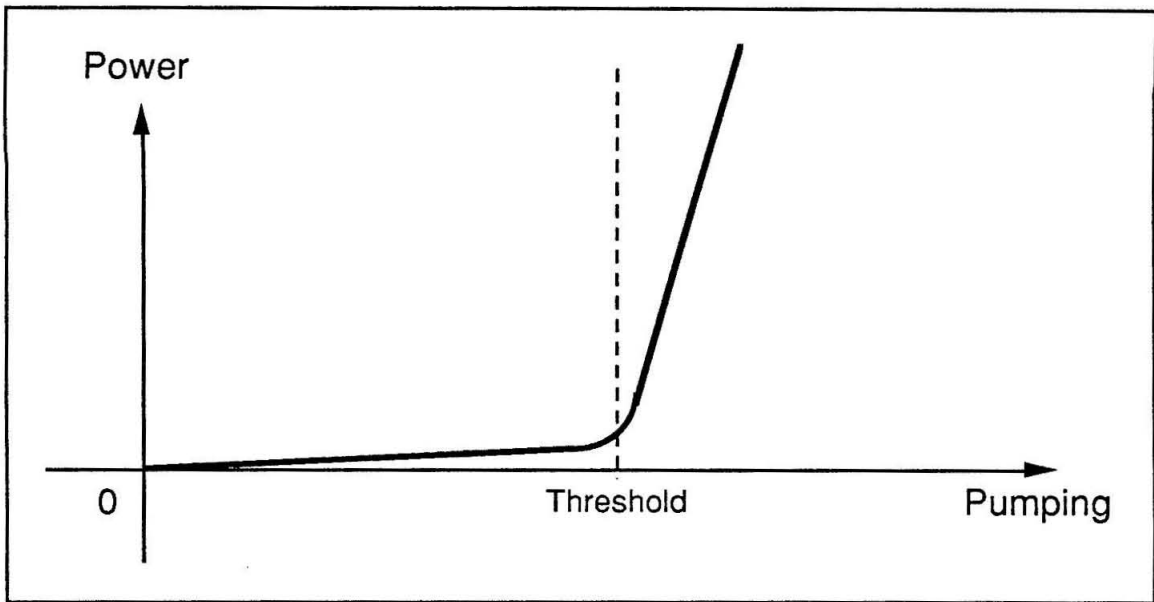


Figure 2.1: The power emitted into the lasing mode versus pumping. The slope undergoes a large sudden increase (by a factor of p) at the threshold point.

p modes. Since p is a large number (typically 10^8), the plot of power emitted into the laser mode versus pumping should have a huge increase in slope at the threshold point [15], see Figure 2.1.

Above threshold, the laser field can be viewed as the sum of:

1. The electric field due to the stimulated emission which has a definite amplitude and phase in time; and
2. the electric field due to spontaneous emission which has a random phase.

The laser noise is mainly a result of the spontaneous emission where the other sources of fluctuations (e.g., fluctuation in pumping) have, for most cases, negligible contributions. The spontaneous emission can be thought of as an “induced transition”

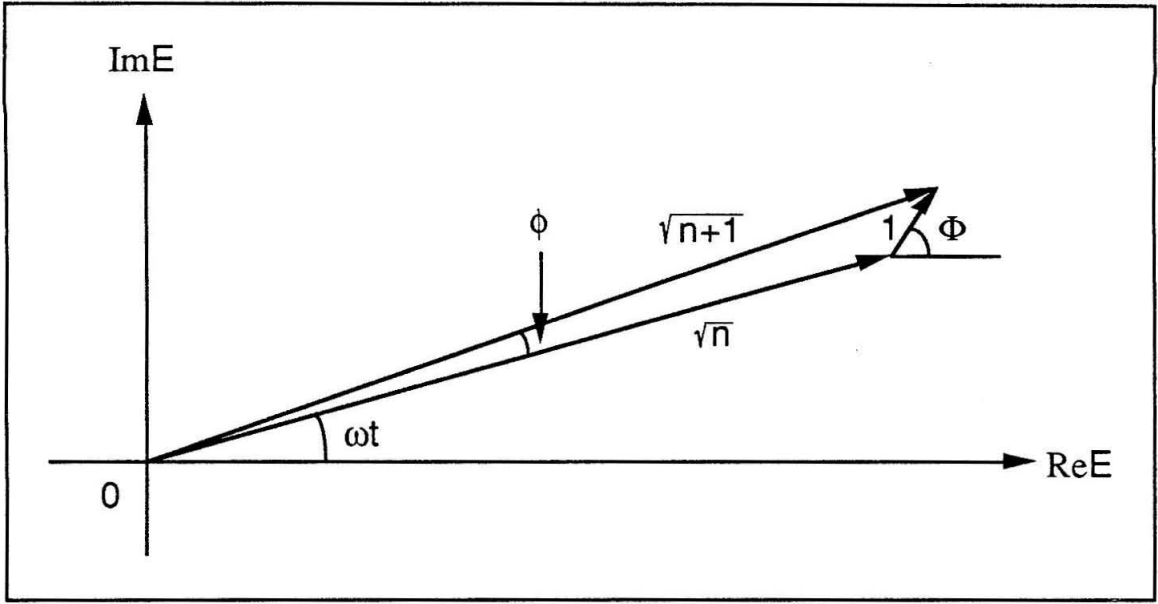


Figure 2.2: The phasor diagram of laser field. The stimulated emission contributes n photons and has a definite phase. The spontaneous emission contributes an additional photon at time t whose phase Φ is random variable between 0 and 2π with a uniform probability distribution. Then the resulting total field at t has a phase equals $\omega t + \phi$.

due to vacuum (zero-point) fluctuation of the radiation field. Because the vacuum is the lowest energy state, conservation of energy allows only the transition of electrons from higher to lower energy states. The quantum mechanical nature of the spontaneous emission makes the laser noise fluctuation a fundamental and inescapable phenomenon.

Consider the phasor diagram of the laser field depicted in Figure 2.2 where at time t a spontaneous emission takes place. The radiation field is the sum of the field due to stimulated emission and that due to the presence of the additional photon caused by spontaneous emission. The field associated with the stimulated emission has an amplitude of \sqrt{n} (n is the number of photons generated by stimulated emission)

and a definite phase ωt at time t , but the field caused by spontaneous emission has an amplitude of unity and a random phase Φ taking values, with equal probability, between 0 and 2π . Consequently, the total optical field has the phase $\omega t + \phi$ at time t where ϕ is a random variable. It is easy to see that the spontaneous emission results in both amplitude and phase fluctuation in laser field. The laser field has, relatively speaking, a significant phase fluctuation and a small amplitude fluctuation due to gain saturation.

To summarize this section, it has been shown that the laser noise fluctuation results mainly from spontaneous emission which is of a quantum mechanical origin.

2.3 Semiclassical Theory of Semiconductor Laser Noise

There are a number of methods to study the problem of laser noise fluctuation [16, 17,18]. A Van der Pol analysis of laser noise is presented in this section. The main references are work by Vahala and Yariv [19,20] and “Quantum Electronics” by A. Yariv [15].

We start with the Maxwell’s equations:

$$\nabla \times \vec{H} = \vec{i} + \frac{\partial \vec{D}}{\partial t} \quad (2.2)$$

$$\nabla \times \vec{E} = -\frac{\partial \vec{B}}{\partial t} \quad (2.3)$$

where for the laser medium under study

$$\vec{D} = \epsilon_0 \vec{E} + \vec{P} \quad (2.4)$$

$$\begin{aligned} \vec{P} &= \vec{P}_{nonresonant} + \vec{P}_{transition} + \vec{p}_{Langevin} \\ &= (\epsilon - \epsilon_0) \vec{E} + \vec{P}_{transition} + \vec{p}_{Langevin} \end{aligned} \quad (2.5)$$

$$\epsilon = \epsilon_0 n^2 \quad (2.6)$$

$$\vec{B} = \mu \vec{H} \quad (2.7)$$

$$\vec{j} = \sigma \vec{E} \quad (2.8)$$

where ϵ_0 and ϵ are vacuum dielectric constant and nonresonant dielectric constant of the laser medium, respectively, n is the nonresonant index of refraction, μ is the magnetic permeability, σ is the medium conductivity, $\vec{P}_{transition}$ is the polarization component due to induced transition which accounts for the laser medium gain, and $\vec{p}_{Langevin}$, the noise source term, is the polarization associated with spontaneous emission.

Solving for \vec{E} , we have

$$\frac{\partial^2 \vec{E}(\vec{r}, t)}{\partial t^2} - \frac{1}{\mu\epsilon} \nabla^2 \vec{E} + \frac{\sigma}{\epsilon} \frac{\partial \vec{E}}{\partial t} = -\frac{1}{\epsilon} \frac{\partial^2}{\partial t^2} (\vec{P} + \vec{p}) \quad (2.9)$$

This equation is the starting point of the Van der Pol analysis.

In the following semiclassical treatment of noise in semiconductor lasers, the electric field is expanded in terms of spatial modes that are solutions of the homogeneous wave equation *with* loss and gain. The mirror reflections are treated as boundary conditions [21].

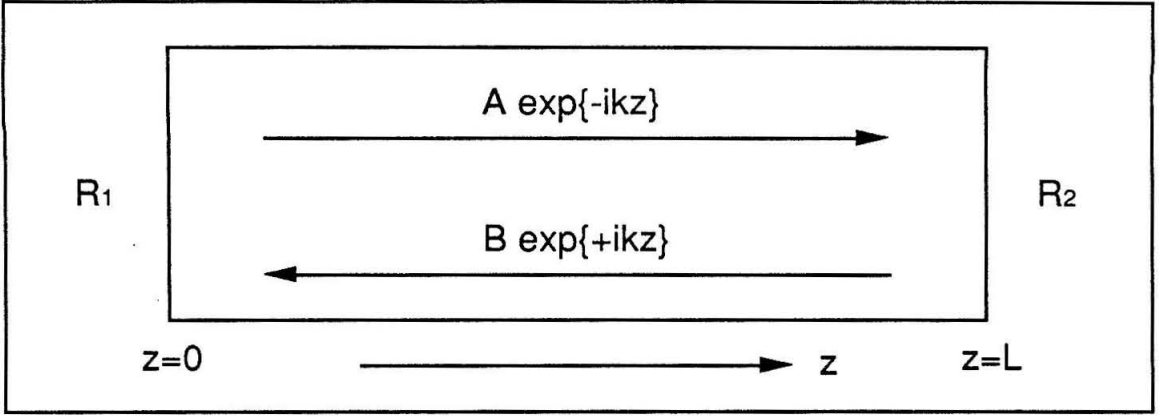


Figure 2.3: A simple semiconductor laser. R_1 and R_2 are facet reflectivities, the electromagnetic wave travels back and forth within the cavity to generate laser oscillation.

Consider a semiconductor laser with end reflections R_1 and R_2 depicted in Figure 2.3. The electric field equals the sum of the left- and right-traveling waves. If there is no spontaneous emission, namely,

$$\vec{p} = 0$$

and for single mode oscillation, we have

$$\vec{E}(\vec{r}, t) \propto \vec{e}(\vec{r}) e^{i\omega_0 t} \quad (2.10)$$

$$\frac{\partial}{\partial t} \rightarrow i\omega_0 \quad (2.11)$$

$$\vec{P} = \epsilon_0 \chi_0 \vec{E} \quad (2.12)$$

Equation 2.9 becomes

$$\frac{d^2}{dz^2} \vec{e} + \omega_0^2 \mu \epsilon_0 n^2 \left(1 + \frac{\chi_0}{n^2} - \frac{i\sigma}{\epsilon_0 n^2 \omega_0} \right) \vec{e} = 0 \quad (2.13)$$

and has a general solution

$$e(\vec{r}) = A e^{-ikz} + B e^{+ikz} \quad (2.14)$$

$$k^2 = \omega_0^2 \mu \epsilon_0 n^2 \left(1 + \frac{\chi_0}{n^2} - \frac{i\sigma}{\epsilon_0 n^2 \omega_0}\right) \quad (2.15)$$

Using the boundary conditions at $z = 0$ and $z = L$, we obtain

$$A = r_1 B \quad (2.16)$$

$$B e^{+ikL} = r_2 A e^{-ikL} \quad (2.17)$$

$$r_1 r_2 e^{-2ikL} = 1 \quad (2.18)$$

where the last equation is the threshold condition and $R_1 = r_1^2$ and $R_2 = r_2^2$. There are many k 's which satisfies Equation 2.18 and each represents a cavity mode.

Now consider the effect of spontaneous emission. The electric field can be generally expanded in terms of the cavity modes that satisfy Equation 2.18

$$\vec{E}(\vec{r}, t) = \sum_m E_m(t) \vec{e}_m(\vec{r}) \quad (2.19)$$

$$\vec{P}(\vec{r}, t) = \sum_m P_m(t) \vec{e}_m(\vec{r}) \quad (2.20)$$

$$\vec{p}(\vec{r}, t) = \sum_m p_m(t) \vec{e}_m(\vec{r}) \quad (2.21)$$

where

$$\nabla^2 \vec{e}_m(\vec{r}) + k_m^2 \vec{e}_m(\vec{r}) = 0 \quad (2.22)$$

$$k_m^2 = \omega_m^2 \mu \epsilon_0 n^2 \left(1 + \frac{\chi_0}{n^2} - \frac{i\sigma}{\epsilon_0 n^2 \omega_m}\right) \quad (2.23)$$

The $E_n(t)$ is governed by the ordinary differential equation

$$\ddot{E}_n + \frac{\sigma}{\epsilon_0 n^2} \dot{E}_n + \omega_n^2 \left(1 + \frac{\chi_0}{n^2} - \frac{i\sigma}{\epsilon_0 n^2 \omega_n}\right) E_n = -\frac{1}{\epsilon_0 n^2} (\ddot{P}_n + \ddot{p}_n) \quad (2.24)$$

where

$$P_n = \epsilon_0 \chi E_n \quad (2.25)$$

$$\chi = \chi^{(1)} + \chi^{(3)}|E_n|^2 \quad (2.26)$$

and $\chi^{(3)}$ is the third order complex susceptibility.

We write

$$E_n(t) = [A_0 + \delta(t)]e^{i[\omega t + \phi(t)]} \quad (2.27)$$

$$p_n(t) = -\frac{1}{\epsilon_0 n^2} \Delta e^{i[\omega t + \phi(t)]} \quad (2.28)$$

where ω is the (average) lasing frequency, $\delta(t)$ and $\phi(t)$ represent the amplitude and phase fluctuations, respectively, and substitute into Equation 2.24, the result is

$$\omega = \omega_n \quad (2.29)$$

$$\dot{\delta} + \omega_1 \delta = \frac{\Delta_i}{2\omega} \quad (2.30)$$

$$A_0 \dot{\phi} - \omega_1 \alpha \delta = -\frac{\Delta_r}{2\omega} \quad (2.31)$$

where

$$\Delta \equiv \Delta_r + i\Delta_i \quad (2.32)$$

$$\omega_1 = -\frac{A_0^2 \chi_i^{(3)}}{n^2} \omega > 0 \quad \text{because} \quad \chi_i^{(3)} < 0 \quad (2.33)$$

$$\alpha = \frac{\chi_r^{(3)}}{\chi_i^{(3)}} < 0 \quad (2.34)$$

The formal solution can be readily obtained by solving the algebraic equations which are the Laplace transforms of Equation 2.30 and 2.31, and performing the inverse Laplace transform. The result is

$$\delta(t) = \frac{1}{2\omega} \int_0^t \Delta_i(\lambda) e^{-\omega_1(t-\lambda)} d\lambda \quad (2.35)$$

$$\Delta\phi(t) = \frac{3\alpha}{4A_0\omega} \left[\int_0^t \Delta_i(\lambda) d\lambda - \int_0^t \Delta_i(\lambda) e^{-\omega_1(t-\lambda)} d\lambda - \frac{1}{2A_0\omega} \int_0^t \Delta_r(\lambda) d\lambda \right] \quad (2.36)$$

where $\Delta\phi(t) \equiv \phi(t) - \phi(0)$. Using the correlations for the random Langevin driving terms [15],

$$\begin{aligned} \langle \Delta_i(\lambda_1) \Delta_i(\lambda_2) \rangle &= \langle \Delta_r(\lambda_1) \Delta_r(\lambda_2) \rangle = Q \delta(\lambda_1 - \lambda_2) \\ \langle \Delta_i(\lambda_1) \Delta_r(\lambda_2) \rangle &= 0 \end{aligned} \quad (2.37)$$

$$Q = \frac{4\hbar\omega_p^3}{\epsilon V \tau_p} \eta \quad (2.38)$$

$$\eta = \left(\frac{N_2}{N_2 - N_1} \right)_{\text{threshold}} \quad (2.39)$$

where τ_p is the photon lifetime. we can calculate the following correlations as

$$\langle \delta(t + \tau) \delta(t) \rangle = \frac{Q e^{-\omega_1 |\tau|}}{8\omega^2 \omega_1} \quad (2.40)$$

$$\langle \Delta\phi(t_1) \Delta\phi(t_2) \rangle = \frac{Q}{4\omega^2 A_0^2} (1 + \alpha^2) \min(t_1, t_2) \quad (2.41)$$

2.4 Laser Spectral Properties

From Equations 2.40 and 2.41, we can calculate all the spectral properties of semiconductor laser.

The field spectrum

The autocorrelation function $C_E(\tau)$ of the laser field is defined as

$$C_E(\tau) = \langle E(t) E(t + \tau) \rangle \quad (2.42)$$

where it is understood that whenever the quadratic form of the field is encountered only the real part of the field is meant. Using results from the last section we have

$$C_E(\tau) = \frac{A_0^2}{2} \Re \langle e^{+i\omega\tau} e^{i\Delta\phi(t,\tau)} \rangle \quad (2.43)$$

$$\Delta\phi(t, \tau) \equiv \phi(t, \tau) - \phi(t) \quad (2.44)$$

The $\langle e^{i\Delta\phi(t,\tau)} \rangle$ factor can be evaluated using Wick's theorem (see Appendix A)

$$\langle e^{i\Delta\phi(t,\tau)} \rangle = e^{-\frac{1}{2}\langle [\Delta\phi(t,\tau)]^2 \rangle} \quad (2.45)$$

Because (see Equation 2.41)

$$\langle [\Delta\phi(t, \tau)]^2 \rangle = \frac{Q}{4\omega^2 A_0^2} (1 + \alpha^2) |\tau| \equiv \frac{2}{\tau_c} |\tau| \quad (2.46)$$

we can calculate the field spectrum and laser linewidth and the results are

$$W_E(\Omega) = \frac{2}{\pi} \int_0^\infty C_E(\tau) e^{-i\omega\tau} d\tau = \frac{A_0^2}{2} \frac{\tau_c/\pi}{1+(\Omega-\omega)^2\tau_c^2} \quad (2.47)$$

$$(\Delta\omega)_{laser} = \frac{2}{\tau_c} = \frac{Q}{4\omega^2 A_0^2} (1 + \alpha^2) \quad (2.48)$$

Using the definition of Q , laser power $P_e = \epsilon A_0^2 v / \tau_p$, and the passive width $(\Delta\nu)_{1/2} = (2\pi\tau_p)^{-1}$, the laser linewidth is

$$(\Delta\nu)_{laser} = \frac{2\pi\hbar\nu\eta(\Delta\nu)_{1/2}^2(1 + \alpha^2)}{P_e} \quad (2.49)$$

so that the laser linewidth is inversely proportional to laser power and directly proportional to the factor $(1 + \alpha^2)$. For solid-state lasers, the laser gain spectrum is symmetric and $\chi_r^{(3)} = 0$ so that $\alpha = 0$. In the case of semiconductor lasers, the stimulated emission is between conduction band and the valence band where α is nonzero

[15]. The measured values of α is approximately 3.5 to 5 [22]. Therefore, the factor $(1 + \alpha^2)$ represents a number between 10 and 30 which contributes, in part, to broad linewidths of semiconductor lasers.

The power fluctuation and frequency spectrum

The laser power is given by

$$P = \frac{\epsilon E^2(t)V}{\tau_p} \quad (2.50)$$

and consequently

$$\Delta P = \frac{2\epsilon V A_0 \delta(t)}{\tau_p} \quad (2.51)$$

Using the results from Section 2.3, we obtain

$$W_{\Delta P}(\Omega) = \frac{4\hbar\omega\eta P_e}{\pi\tau_p^2} \left(\frac{1}{\Omega^2 + \omega_1^2} \right) \quad (2.52)$$

Similarly the frequency fluctuation spectrum can be evaluated as

$$W_{\Delta\omega}(\Omega) = \frac{\eta\hbar\omega}{\pi\tau_p^2 P_e} \left(\frac{\alpha}{\Omega^2 + \omega_1^2} \right) \quad (2.53)$$

where the instantaneous frequency is defined as

$$\omega(t) = \omega + \dot{\phi}(t) \quad (2.54)$$

The basic features of $W_{\Delta\omega}(\Omega)$ were verified experimentally by Mannes and Siegman [23].

2.5 Intra-Cavity Dispersive Medium

Semiconductor lasers have generally a broad linewidth. A good commercial semiconductor laser typically has a $10 \sim 20 \text{ MHz}$ linewidth. In some coherent communication applications, it is desirable to have a narrower linewidth (longer coherence time) semiconductor laser as a coherent light source. Various linewidth reduction schemes are available. In this section a semiconductor laser with an intra-cavity medium with dispersive response [24] is studied for the purpose of understanding how linewidth reduction occurs.

In Equation 2.9, if we make the substitution

$$\frac{\sigma}{\epsilon} \rightarrow \frac{\sigma}{\epsilon} + 2C\dot{\phi}(t) \quad (2.55)$$

i.e., in addition to normal optical loss, the laser cavity contains a dispersive medium which responds to the instantaneous frequency of the laser field. The constant C can be complex whose real part is associated with a gain or loss and the imaginary part is due to frequency dependent phase delay.

Equations 2.30, and 2.31 become

$$\dot{\delta} + \omega_1\delta + A_0C_r\dot{\phi} = \frac{\Delta_i}{2\omega} \quad (2.56)$$

$$A_0(1 + C_i)\dot{\phi} - \omega_1\alpha\delta = -\frac{\Delta_r}{2\omega} \quad (2.57)$$

where

$$C \equiv C_r + iC_i \quad (2.58)$$

The primary consequences of introducing this dispersive medium are demonstrated

in the following results

$$\langle \delta(t + \tau)\delta(t) \rangle = \frac{Q}{8\omega^2\omega_1} \frac{(1+C_i)^2+C_r^2}{(1+C_i)(1+C_i+\alpha C_r)} e^{-\omega_1(1+\frac{\alpha C_r}{1+C_i})|\tau|} \quad (2.59)$$

$$\langle \Delta\phi(t_1)\Delta\phi(t_2) \rangle = \frac{Q}{4\omega^2 A_0^2} \frac{(1+\alpha^2)}{(1+C_i+\alpha C_r)^2} \min(t_1, t_2) \quad (2.60)$$

$$W_{\Delta P}(\Omega) = \frac{4\hbar\omega\eta P_e}{\pi\tau_p^2} \frac{(1+C_i)^2+C_r^2}{(1+C_i)^2\Omega^2+\omega_1^2(1+C_i+\alpha C_r)^2} \quad (2.61)$$

$$(\Delta\nu)_{laser} = \frac{2\pi\hbar\nu\eta(\Delta\nu)_{1/2}^2}{P_e} \frac{(1+\alpha^2)}{(1+C_i+\alpha C_r)^2} \quad (2.62)$$

The following observations are made:

1. The presence of dispersive medium in semiconductor laser can have a dramatic impact on laser spectral behavior. The correct sign of C leads to linewidth reduction, amplitude fluctuation suppression, and an increase in relaxation resonance frequency. The wrong sign would result in the opposite.
2. The laser linewidth is reduced by a factor of

$$(1 + C_i + \alpha C_r)^2$$

when $\alpha C_r \gg 1$ and the linewidth is lower than the Schawlow-Townes limit [25] (when $\alpha = 0$) by a factor of C_r^2 which means the laser benefits from nonzero value of the “old devil” α .

3. When $\alpha = 0$ (as in solid-state lasers, etc.), the dispersive loss (C_r) has no effects on laser linewidth (since there is no amplitude-to-phase coupling), but the dispersive phase response (C_i) does and actually results in linewidth reduction by a factor of $(1 + C_i)^2$ for $C_i > 0$ or $C_i < -2$.

4. Amplitude fluctuation is reduced when

$$\frac{\alpha C_r}{1 + C_i} > 0$$

because of higher damping rate.

5. Notice that in the last section the laser frequency fluctuation spectrum has an “at half maximum frequency” of ω_1 . Now it is replaced by

$$\omega_1 \rightarrow \omega_1 \left(1 + \frac{\alpha C_r}{1 + C_i}\right)$$

therefore, one should expect the maximum modulation frequency to increase by

$$1 + \frac{\alpha C_r}{1 + C_i}$$

To conclude this section, it is shown that a dispersive medium within a laser cavity can lead to significant linewidth reduction, enhancement of modulation response, and suppression of intensity fluctuation when C is properly chosen. Although the analysis deals with a intra-cavity dispersive medium, a proper modification can extend this analysis to the case of dispersive external feedback.

2.6 Semiconductor Laser Exposed to External Optical Feedbacks

One of the important reasons the external optical feedback is introduced to a semiconductor laser is for the purpose of reducing the laser linewidth. Experimentally

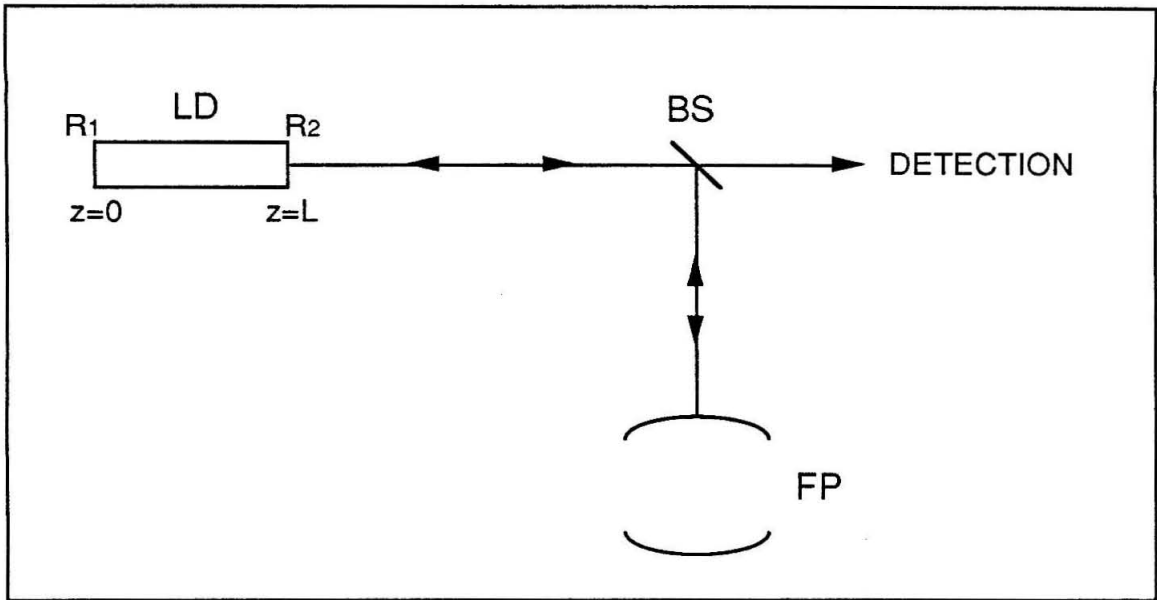


Figure 2.4: A semiconductor laser exposed to external feedback from a Fabry-Perot etalon.

it is observed that semiconductor lasers are very sensitive to optical feedback even at very weak levels ($10^{-3} \sim 10^{-4}$) and large reductions in linewidth can be obtained when external feedback is properly tuned [26].

The spectral behavior of semiconductor lasers exposed to external feedback can be dealt with in the context of rate equations [26]. It is the purpose of this section to tackle the problem in the context of the Maxwell wave equations and treat the external optical feedback as dispersive reflection at the facet where the feedback is introduced [21]. The advantage of the Maxwell equation approach is that it is fundamental and the $1 + \alpha^2$ dependence in laser linewidth arises naturally in contrast to the rate equation approach.

Consider a semiconductor laser exposed to external feedback from a Fabry-Perot

(FP) etalon depicted in Figure 2.4. The traveling time between the laser and the FP is much shorter than the time scale on which the laser phase fluctuates. Therefore, one can treat the feedback as part of the (instantaneous) reflection with a proper phase delay. From this standpoint, the problem effectively is reduced to that of a single section laser with a frequency dependent one facet reflection coefficient.

First, the reflection from a FP (with cavity length l and mirror reflection coefficient r) is given by

$$\frac{\text{Reflection}}{\text{Incident}} = r \frac{1 - e^{-2ik_0l}}{1 - Re^{-2ik_0l}} \quad (2.63)$$

where

$$R = r^2 \quad (2.64)$$

$$k_0 = \frac{\omega_{\text{incident}}}{c} \quad (2.65)$$

The additional reflection due to feedback at the second facet of the laser (see Figure 2.4) is then given by

$$\Delta r_2 = \sqrt{\eta_c}(1 - R_2)e^{-2ik_0L_0}r \frac{1 - e^{-2ik_0l}}{1 - Re^{-2ik_0l}} \quad (2.66)$$

where η_c is the feedback intensity coupling factor, R_2 is the reflectivity of the second laser facet, and L_0 is the distance between the second facet and the FP. The feedback from a FP has a characteristic that its value can change sharply within a narrow frequency range.

For an incident beam with instantaneous frequency

$$\omega(t) = \omega + \dot{\phi}(t)$$

we have

$$k_0 \rightarrow k_0 + \frac{\dot{\phi}}{c} \quad (2.67)$$

$$\Delta r_2[\omega(t)] = \Delta r_2(\omega) + \sqrt{\eta_c}(1 - R_2)e^{-2ik_0L_0} \frac{\dot{\phi}l}{c(1-R)} \quad (2.68)$$

where the reflection from the FP equals $\frac{1}{2}$ has been chosen as the operating point.

The mirror reflection is a discrete optical loss (concentrated at one place) while the σ/ϵ represents the medium loss which is distributed. Since we consider the fluctuations on the time scale that is much longer than the cavity round trip time, they (mirror reflection and medium loss) are essentially equivalent. Therefore, the additional reflection can be absorbed in the distributed loss term. Using the relationships

$$\text{total loss} = \alpha - \frac{1}{L} \ln(r_1 r_2) \quad (2.69)$$

$$\frac{\sigma}{\epsilon} = \frac{c\alpha}{n} \quad (2.70)$$

it can be seen that to include the feedback the following substitution must be made

$$\frac{\sigma}{\epsilon} \rightarrow \frac{\sigma}{\epsilon} - \frac{c}{nL} \frac{\Delta r_2}{r_2} \quad (2.71)$$

$$\rightarrow \frac{\sigma}{\epsilon} - \frac{l}{nL} \frac{1 - R_2}{\sqrt{R_2}(1 - R)} \sqrt{\eta_c} e^{-2ik_0L_0} \dot{\phi} \quad (2.72)$$

The C parameter defined by Equation 2.55 in this case is given by

$$C = -\frac{l}{2nL} \frac{1 - R_2}{\sqrt{R_2}(1 - R)} \sqrt{\eta_c} e^{-2i\omega L_0/c} \quad (2.73)$$

where l and L are lengths of FP and laser cavities, respectively, n is laser medium index, ω is lasing frequency, R and R_2 are reflectivities of FP mirror and second laser

facet, respectively, L_0 is the distance between FP and the laser, and η_c is the feedback coupling factor.

One interesting observation is that one can always adjust L_0 to make C real and have the correct sign (negative) for noise reduction. Furthermore, a numerical estimate shows that the C is typically $\sim 20 - 30$ such that $|\alpha C|$ is much greater than unity. Hence, according to Equation 2.62, regardless the sign of C a reduction in linewidth will always result.

2.7 References

- [1] N. G. Basov, O. N. Krokhin, and Y. M. Popov, *J.E.T.P.*, **40**, 1320(1961).
- [2] R. N. Hall, G. E. Fenner, J. D. Kingsley, T. J. Soltys, and R. O. Carlson, *Phys. Rev. Lett.*, **9**, 366(1962).
- [3] M. I. Nathan, W. P. Dumke, G. Burns, F. H. Dills, and G. Lasher, *Appl. Phys. Lett.*, **1**, 62(1962).
- [4] Z. I. Alferov, et al., *Sov. Phys.—Semicon.*, **4**, 1573(1971).
- [5] J. M. Hayashi, M. B. Panish, and P. W. Foy, *IEEE J. Quant. Elec.*, **QE-5**, 211(1969).
- [6] H. Kressel and H. Nelson, *RCA REv.*, **30**, 106(1969).
- [7] W. W. Anderson, *IEEE J. Quant. Elec.*, **QE-1**, 228(1965).
- [8] H. Kressel and J. K. Butler, *Semiconductor Lasers and Heterojunction on LED's*, Academic Press, New York, 1977.
- [9] J. P. van der Ziel, R. Dingle, R. C. Miller, W. Wiegmann, and W. A. Nordland, Jr., *Appl. Phys. Lett.*, **26**, 463(1975).
- [10] R. D. Dupuis, P.D. Dapkus, *IEEE J. Quant. Elec.*, **QE-16**, 170(1980).
- [11] P. Derry, et al., *Appl. Phys. Lett.*, **50**, 1773(1987).

- [12] S. C. Kan, S. Wu, S. Sanders, G. Griffel, and A. Yariv, *J. Appl. Phys.*, **69**, 3384(1991).
- [13] S. C. Kan, S. Sanders, G. Griffel, G. H. Lang, S. Wu, and A. Yariv, *Appl. Phys. Lett.*, **58**, 1548(1991).
- [14] I. Grave, S. C. Kan, G. Griffel, S. Wu, A. Sa'ar, and A. Yariv, *Appl. Phys. Lett.*, **58**, 110(1991).
- [15] A. Yariv, *Quantum Electronics*, 3rd ed. (John Wiley & Sons, New York, 1989).
- [16] M. Lax and W. H. Louisell, *IEEE J. Quant. Elec.*, **QE-3**, 47(1967).
- [17] M. Lax, *Phys. Rev.*, **157**, 213(1967).
- [18] C. H. Henry, *IEEE J. Quant. Elec.*, **QE-18**, 259(1982).
- [19] K. Vahala and A. Yariv, *IEEE J. Quant. Elec.*, **QE-19**, 1096(1983).
- [20] K. Vahala and A. Yariv, *IEEE J. Quant. Elec.*, **QE-19**, 1102(1983).
- [21] S. Wu and A. Yariv, "A theoretical investigation of linewidth reduction in three section distributed-feedback laser," in preparation.
- [22] C. Harder, K. Vahala, and A. Yariv, *Appl. Phys. Lett.*, **42**, 328(1983).
- [23] K. R. Mannes and A. E. Siegman, *Phys. Rev.*, **4**, 373(1971).
- [24] A. Yariv, R. Nabiev, and K. Vahala, to be published.
- [25] L. Schawlow and C. H. Townes, *Phys. Rev.*, **112**, 1940(1958).

- [26] P. H. Laurent, A. Clairon, and C. H. Breaud, *IEEE J. Quant. Elec.*, **25**, 1131(1989).

Chapter 3

Theory of Monolithic

Semiconductor Laser Linewidth

Reduction

In Section 2.6, drastic linewidth reduction is predicted to result when using external optical feedback. A more aggressive goal is to accomplish such feedback monolithically. In this chapter, a monolithic linewidth reduction scheme is proposed and analyzed. The result will show that under proper pumping and biasing conditions, the multiple section semiconductor distributed-feedback (DFB) lasers can attain very narrow linewidth [1].

3.1 A Simplified Model

From Sections 2.5 and 2.6, it is understood that the essential requirement for linewidth reduction to occur is to have a dispersive (frequency-dependent) element in the laser system. The intra-cavity dispersive medium serves as a self-quenching mechanism against noise fluctuation while external optical feedback works as a negative feedback similar to the electronic counterpart. Both greatly stabilize the noise fluctuation and narrower linewidths result.

To monolithically implement such a dispersive element induced noise suppression scheme in semiconductor lasers, naturally a multiple section laser is required. In this section a simple idea is explored and serves as a start-up exercise for a realistic approach later.

Let us consider a two section semiconductor laser, depicted in Figure 3.1, with individual section lengths L_1 and L_2 . Each is pumped with direct current injections. In addition to the facet reflections at both ends, an imagined reflection is introduced at $z = 0$ [1].

The electric field is the sum of left- and right-traveling waves, where

$$k_i^2 = \omega_0^2 \mu \epsilon_0 n^2 \left(1 + \frac{\chi_{0i}}{n^2} - \frac{i\sigma}{\epsilon_0 n^2 \omega_0} \right) \quad (3.1)$$

$$i = 1, 2$$

and the threshold condition is determined by the following boundary conditions

$$Ae^{+ik_1L_1} = r_1Be^{-ik_1L_1} \quad (3.2)$$

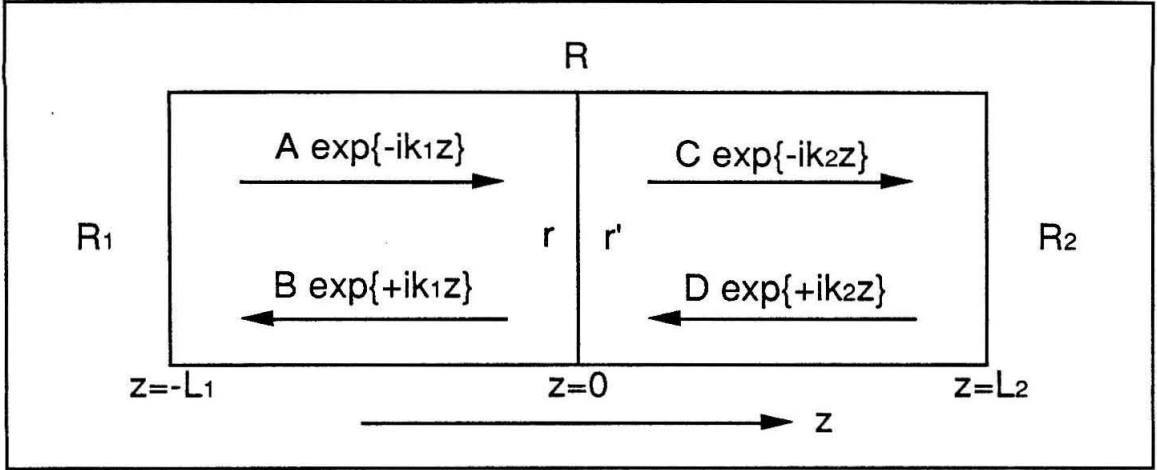


Figure 3.1: A two section semiconductor laser. Both sections are pumped and an imagined reflection is introduced at $z = 0$.

$$De^{+ik_2L_2} = r_2Ce^{-ik_2L_2} \quad (3.3)$$

$$B = rA + t'D \quad (3.4)$$

$$C = tA + r'D \quad (3.5)$$

where r , r' , t , and t' are the corresponding reflection and transmission coefficients at $z = 0$. Define

$$\beta_i \equiv k_i L_i \quad (3.6)$$

and look for nonzero solutions of the boundary conditions, the threshold condition is obtained as

$$1 - r_1 r e^{-2i\beta_1} - r_2 r' e^{-2i\beta_2} + r_1 r_2 (r r' - t t') e^{-2i(\beta_1 + \beta_2)} = 0 \quad (3.7)$$

From the cavity 1 standpoint, the effective reflection at $z = 0$ is given by

$$r_{eff} \equiv \frac{B}{A} = r + \frac{r_2 t t' e^{-2i\beta_2}}{1 - r_2 r' e^{-2i\beta_2}} \quad (3.8)$$

which is the original reflection coefficient r due to the imagined mirror plus additional reflection Δr_{eff} resulting from the feedback from the second cavity. Δr_{eff} has a characteristic that is typical of a FP-like reflection coefficient

$$\frac{1}{1 - r_2 r' e^{-2i\beta_2}}$$

where for a high finesse FP the denominator can be a very small number when the frequency is appropriately chosen. If the second cavity is unpumped, then the fraction is a number comparable in magnitude to unity independent of the frequency because

$$|r_2 r' e^{-2i\beta_2}| = |r_2 r' e^{-\alpha L_2}| < 1$$

where α is the medium loss coefficient. When the second cavity possesses gain (just below its threshold), then

$$|r_2 r' e^{-2i\beta_2}| = |r_2 r' e^{(\gamma - \alpha)L_2}|$$

can be brought very close to unity, where γ is the medium gain coefficient. Thus, a carefully pumped second cavity will simulate a high finesse FP. Of course, an active element will also generate spontaneous emission whose effect will be addressed later in this section.

Let us consider two extreme cases

1. For 100% coupling between the two cavities, we have following equations

$$r = r' = 0, \quad t = t' = 1$$

$$r_1 r_2 e^{-2i(\beta_1 + \beta_2)} = 1$$

Therefore, the two section structure becomes a simple laser with nonuniform pumping.

2. For no coupling between the two cavities

$$r = r' = 1, \quad t = t' = 0$$

$$r_1 e^{-2i\beta_1} = 1$$

$$r_2 e^{-2i\beta_2} = 1$$

Thus, the two section structure becomes two separate lasers which are completely uncoupled.

Now we consider the effect of a slowly (relatively speaking) varying frequency on the r_{eff} which depends on the frequency through the factor

$$e^{-2i\beta_2} = e^{-2i(\beta_{20} + \frac{n\dot{\phi}}{c}L_2)}$$

where

$$\omega(t) = \omega + \dot{\phi}$$

Using realistic values of $L_2 \sim 300\mu m$, $n = 3.5$, and $\dot{\phi} < 2\pi \times 100MHz$, we have

$$\frac{n\dot{\phi}}{c}L_2 < 10^{-4} \quad (3.9)$$

A straightforward calculation shows that [1]

$$r_{eff}[\omega(t)] = r_{eff}(\omega) + \Delta r_{eff} \quad (3.10)$$

$$\frac{\Delta r_{eff}}{r_{eff}} = 2i\left(\frac{n\dot{\phi}}{c}L_2\right)(R_2 t t') \left(\frac{e^{-2i\beta_{20}}}{1 - r_2 r' e^{-2i\beta_{20}}}\right)^2 \dot{\phi} \quad (3.11)$$

$$\frac{\sigma}{\epsilon} \rightarrow \frac{\sigma}{\epsilon} - 2iR_2tt' \left(\frac{L_2}{L_1}\right) \left(\frac{e^{-2i\beta_{20}}}{1-r_2r'e^{-2i\beta_{20}}}\right)^2 \dot{\phi} \quad (3.12)$$

$$C = -iR_2tt' \left(\frac{L_2}{L_1}\right) \left(\frac{e^{-2i\beta_{20}}}{1-r_2r'e^{-2i\beta_{20}}}\right)^2 \quad (3.13)$$

where the C parameter as defined in Equation 2.55 can be a large number, even in the weak feedback regime, when the second cavity is properly pumped just below its own threshold, i.e., when

$$r_2r'e^{-2i\beta_{20}} \approx 1 \quad (3.14)$$

The second cavity not only results in a large C which is what is desired, but also contributes additional noise due to its own spontaneous emission. This generates an additional random radiation field. For a single section laser, its effect is treated as the Langevin noise source term which represents the random polarization [2,3,4]. In our case the first cavity is driven by its own spontaneous emission and the noise generated in the second cavity then subsequently enters the first cavity. These two noise sources have the same physical nature (both are due to spontaneous emission) and the only difference is that one is generated within the cavity and the other is generated exterior to the cavity and is subsequently coupled into the main cavity. Since we consider noise fluctuation on the time scale that is much larger than the time scales of spontaneous emission and the propagation, they *can* be treated on the same footing. This amounts to a minor renormalization (a factor of $\sim 2 - 3$, depends on pumping, etc.) of the noise power parameter Q [1]. The same conclusion can be drawn if one treats the two-cavity laser as one system where spontaneous emission in two cavities are represented by a single random polarization term. The key is the

difference in time scales. In the single section laser, we are not usually concerned where individual spontaneous emission takes place and treat it collectively [2,3,4] precisely because of different time scales.

To conclude this section, it has been shown that a two section laser, with an imagined mirror separating them, can be viewed effectively as a semiconductor laser with external feedback. The additional noise introduced at the second cavity will merely renormalize the quantity Q .

3.2 Distributed-Feedback Lasers

In the last section we discussed linewidth reduction by employing a two section laser with an imagined mirror reflection between each. In actual devices, such a physical reflection does not exist. Fortunately, the distributed-feedback (DFB) lasers [5] provide a solution. In a DFB laser, the grating can be viewed as many distributed small reflectors (mirrors). With sufficient gain by direct current pumping, a DFB laser can produce laser action without facet reflections [6,4]. In this section, we will examine some of the basic results for a simple DFB laser which will be used in the next section where three section DFB lasers are considered.

A DFB laser is simply a typical semiconductor laser with periodic dielectric constant along the laser cavity. The dielectric periodicity is due to a corrugation formed by physical etching. The electric field inside the laser can, again, be viewed as the

sum of oppositely traveling waves

$$E(z, t) = e(z) e^{i\omega t} \quad (3.15)$$

$$e(z) = A(z) e^{+i\beta' z} + B(z) e^{-i\beta' z} \quad (3.16)$$

where

$$\beta' \equiv \beta + i\gamma \quad (3.17)$$

$$\gamma \equiv \gamma_0 - \alpha \quad (3.18)$$

β is the propagation constant, γ_0 is the gain coefficient, and α is the optical loss. The $A(z)$ and $B(z)$ coefficients are governed by the coupled-mode equations

$$\frac{dA}{dz} = \kappa B e^{-2i(\Delta\beta + i\gamma)z} \quad (3.19)$$

$$\frac{dB}{dz} = \kappa^* A e^{+2i(\Delta\beta + i\gamma)z} \quad (3.20)$$

where

$$\Delta\beta \equiv \beta - \beta_0 = \beta - \frac{l\pi}{\Lambda} \quad (3.21)$$

$$l = \text{integer}$$

and Λ is the grating period. We consider a DFB section of length L and want to calculate the reflection and transmission coefficients. The primary results are given as the following:

1. For laser light incident from the left ($A(L) = 0$)

$$r_L = \frac{-\kappa \sinh(SL)}{S \cosh(SL) - (\gamma - i\Delta\beta) \sinh(SL)} \quad (3.22)$$

$$t_L = \frac{S e^{-i\beta_0 L}}{S \cosh(SL) - (\gamma - i\Delta\beta) \sinh(SL)} \quad (3.23)$$

where

$$S^2 = \kappa^2 + (\gamma - i\Delta\beta)^2 \quad (3.24)$$

and κ is the mode coupling constant.

2. For laser light incident from the right ($B(0) = 0$)

$$r_R = \frac{\kappa^* \sinh(SL) e^{-2i\beta_0 L}}{S \cosh(SL) - (\gamma - i\Delta\beta) \sinh(SL)} \quad (3.25)$$

$$t_R = \frac{S e^{-i\beta_0 L}}{S \cosh(SL) - (\gamma - i\Delta\beta) \sinh(SL)} \quad (3.26)$$

The laser threshold condition is obtained by setting the denominator in the above equations to zero, and the result is

$$\tanh(SL) = \frac{S}{\gamma - i\Delta\beta} \quad (3.27)$$

The above results were obtained assuming no reflection from either facet.

3.3 Multiple Section Distributed-Feedback Lasers

There are a number of research groups which reported on multiple section DFB lasers for linewidth reduction. Some used inhomogeneous pumping, phase shifting between sections [7,8], and others employed different grating periods in different sections. They achieved significant linewidth reduction and the narrowest linewidth reported was 170kHz in a monolithic structure [9].

In this section, three section DFB laser structures are proposed and analyzed for laser linewidth reduction [1]. The basic idea is quite different from that of other

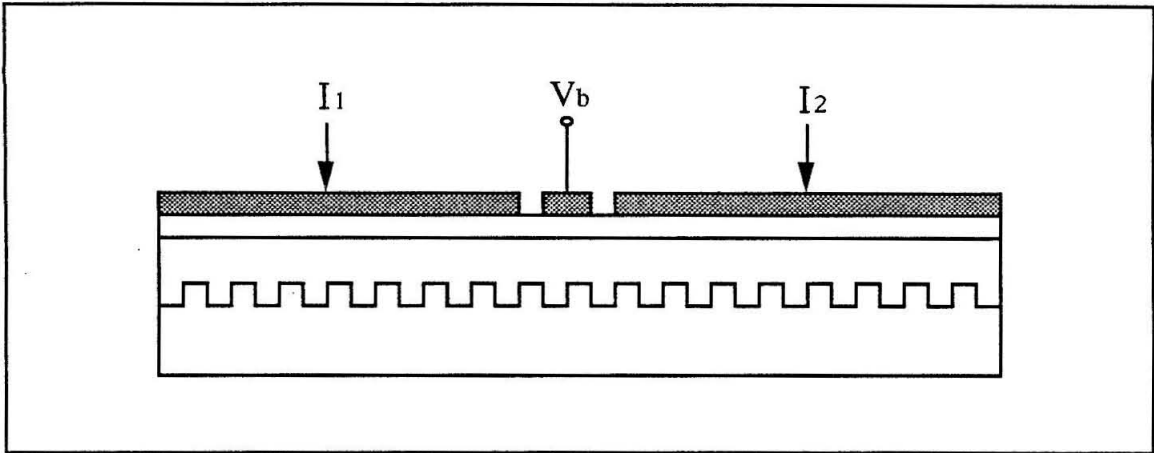


Figure 3.2: A three section DFB laser structure. The middle section is short and reverse biased. The first cavity is pumped above its threshold providing laser action while the second cavity is pumped just below its threshold providing proper feedback for the first cavity.

schemes. Instead of simply pumping inhomogeneously in different sections, a three section structure with a short and highly absorptive middle section (achieved by a reverse bias) is proposed. The first end section is operated above its threshold to provide lasing while the second end section is pumped just below its threshold to simulate a high finesse Fabry-Perot (FP) etalon. The presence of the highly absorptive middle section effectively separates the two end sections and only weak coupling is allowed. It is essential to pump the second cavity properly such that it will provide the FP-like weak feedback to the first end section.

In Sections 3.1, and 3.2, we have laid the ground work for this section so that some of the concepts and results will be directly used. Consider the proposed three section DFB structure, depicted in Figure 3.2. By pumping and biasing, the structure is naturally divided into three cavities with the middle cavity purely absorptive. We

treat the first cavity as an individual DFB laser and represent the impact of the other two sections by effective frequency dependent reflection. Let us imagine a cross section plane in the middle of the first cavity where two reflection coefficients can be defined: One for incidence from the left r_1 , and the other for incidence from the right r_2 . Using the results from Section 3.2, they are calculated as following:

$$r_2 = \frac{\kappa^* \sinh(\frac{S_1 L_1}{2}) e^{-i\beta_0 L_1}}{S_1 \cosh(\frac{S_1 L_1}{2}) - (\gamma_1 - i\Delta\beta) \sinh(\frac{S_1 L_1}{2})} \quad (3.28)$$

$$r_1 = \frac{-\kappa \sinh(\frac{S_1 L_1}{2}) e^{+i\beta_0 L_1}}{S_1 \cosh(\frac{S_1 L_1}{2}) - (\gamma_1 - i\Delta\beta) \sinh(\frac{S_1 L_1}{2})} \quad (3.29)$$

where the second equation holds when there is no feedback from the second cavity, and subscripts 1 and 2 indicate first and second cavities, respectively.

To include the effect of the feedback, the successive transmission and reflection coefficients must be calculated using the results from the last section. Then some simplification is made using the threshold condition. After some algebraic manipulation, eventually we obtain

$$r_1 \rightarrow r_1 \left(1 + \frac{\Delta r_1}{r_1}\right) \quad (3.30)$$

$$\frac{\Delta r_1}{r_1} = \frac{S_1^2 e^{-(\alpha+2i\Delta\beta)a}}{\kappa \sinh^2(\frac{S_1 L_1}{2})} \frac{\sinh(S_2 L_2)}{S_2 \cosh(S_2 L_2) - (\gamma_2 - i\Delta\beta) \sinh(S_2 L_2)} \quad (3.31)$$

where a is the middle section length.

Although the derivation of a close analytic expression of C parameter as defined in Section 2.5 is straightforward but a formidable task, even if accomplished, to obtain the desired numerical estimate would be difficult. Therefore, the following calculation was carried out.

First a few facts need to be understood. Obviously C is linearly proportional to the (amplitude) feedback level, however, this only provides limited help in terms of obtaining large C . Excessive feedback in semiconductor laser will result in chaotic behavior of the laser [10,11,12] and, therefore, only to a degree, can larger C be obtained by simply increasing the optical feedback. It is a very interesting subject to study the chaotic behavior of the multiple section DFB laser in the medium to high feedback regime and it is the author's prejudice that a proper device with *controllable* chaos will be essential in future information processing especially decision making. However, the chaotic behavior of multiple section DFB lasers is beyond the scope of this thesis. In any event, we are limited by the maximum allowable optical feedback of the semiconductor lasers and merely increasing the feedback level does not produce the desired results.

If the semiconductor laser is operating at the maximum allowable feedback level, what else can be attempted to increase C ? The second fact that needs to be understood is that the C parameter is linearly proportional to the first derivative of the optical feedback with respect to laser frequency. Based on these two facts, the performance of the three section device can be compared to that of a semiconductor laser exposed to external feedback from a high finesse FP etalon. Each feedback scheme has a FP-like response factor, f_{FP} , in the expression of the feedback. We only need to compare

$$\frac{1}{f_{FP}} \frac{df_{FP}}{d\omega}$$

and is demonstrated as follows.

1. In the case of external feedback from a FP etalon, we have

$$f_{FP} = \frac{1 - e^{-2ikL_{FP}}}{1 - Re^{-2ikL_{FP}}} \quad (3.32)$$

$$\frac{1}{f_{FP}} \frac{df_{FP}}{d\omega} = \frac{\sqrt{2}L_{FP}}{c(1-R)} \quad (3.33)$$

Using realistic values that $L_{FP} = 10cm$, and $1 - R = 0.01$, one has

$$\frac{1}{f_{FP}} \frac{df_{FP}}{d\omega} \simeq 5 \times 10^{-8} \text{seconds} \quad (3.34)$$

2. For the three section DFB laser, from Equation 3.31, we have

$$f_{FP} = \frac{\kappa \sinh(S_2 L_2)}{S_2 \cosh(S_2 L_2) - (\gamma_2 - i\Delta\beta) \sinh(S_2 L_2)} \quad (3.35)$$

$$\frac{1}{f_{FP}} \frac{df_{FP}}{d\omega} = -i f_{FP} \kappa^{-1} \frac{n}{c} \sim -i f_{FP} \frac{nL_2}{c} \quad (3.36)$$

The result appears strikingly similar in the two cases. For an order of magnitude estimate, we notice that in the case of a three section DFB laser, L_{FP} is replaced by nL_2 which results in C being reduced in magnitude by a factor of 50. This has to do with the simple physics that f_{FP} factor and, hence, the feedback, varies with changing frequency through the phase delay in the second cavity. The smaller the cavity length, the smaller the phase delay variation with constant frequency change. However, the f_{FP} factor in the three section DFB laser can be, at least theoretically, arbitrarily large. It is not difficult to obtain $f_{FP} = 100$ in actual devices so a C of the order unity is within reasonable reach which would result, according to Section 2.5, in a linewidth reduction factor of $10 \sim 20$. To achieve much larger reduction, as in the external feedback case, we need to pump the second cavity very close to its threshold

and achieve mode matching between the first and second cavities. Ideally the first section should and can be made a tunable laser which would result in easily achieved mode matching. Another method to optimize linewidth reduction is to operate at the maximum allowable feedback level and there are simple considerations [13] which can be used to make a DFB laser more tolerable of optical feedback.

To summarize this chapter, it has been demonstrated that the three section DFB lasers can reach significant linewidth reduction by proper pumping and biasing. The middle section has to be short and highly absorptive. The first end section should be pumped above its threshold to provide lasing while the other end section should be pumped very close to its threshold. A linewidth reduction on the order of $10 \sim 20$ should be within reasonable reach based upon numerical estimates. Potentially drastic linewidth reductions can be obtained by very careful pumping and mode matching.

3.4 References

- [1] S. Wu and A. Yariv, "A theoretical investigation of linewidth reduction in three section distributed-feedback lasers," in preparation.
- [2] K. Vahala and A. Yariv, *IEEE J. Quant. Elec.*, **QE-19**, 1096(1983).
- [3] K. Vahala and A. Yariv, *IEEE J. Quant. Elec.*, **QE-19**, 1102(1983).
- [4] A. Yariv, *Quantum Electronics*, 3rd ed. (John Wiley & Sons, New York, 1989).
- [5] M. Nakamura, A. Yariv, H. W. Yen, S. Somekh, and H. L. Garvin, *Appl. Phys. Lett.*, **22**, 515(1973).
- [6] M. Nakamura, W. H. Yen, A. Yariv, E. Garmire, S. Somekh, and H. L. Garvin, *Appl. Phys. Lett.*, **23**, 224(1973).
- [7] Y. Kotaki, et al., *Electron. Lett.*, **25**, 990(1989).
- [8] M. Kitamura, et al., *IEEE Photon. Tech. Lett.*, **2**, 310(1990).
- [9] M. Okai, T. Tsuchiya, K. Uomi, N. Chinone, and T. Harada, *IEEE Photon. Tech. Lett.*, **2**, 529(1990).
- [10] J. Sacher, W. Elsässer, and E. O. Göbel, *Phys. Rev. Lett.*, **63**, 2224(1989).
- [11] B. Tromborg and J. Mørk, *IEEEJ. Quant. Elec.*, **26**, 642(1990).
- [12] J. Mørk, J. Mark, and B. Tromborg, *Phys. Rev. Lett.*, **65**, 1999(1990).
- [13] T. Kurosaki, T. Hirono, and M. Fukuda, presented at *OFC'92*, paper FB4.

Chapter 4

Experimental Study of Multiple Section Distributed-Feedback Semiconductor Lasers

4.1 DFB Laser Structure

Distributed-feedback lasers [1,2] are the primary commercial semiconductor laser sources for many practical applications because of their single mode operation. One of the key factors to obtaining high performance DFB lasers is to confine the current to a narrow active region. Therefore, a lateral current confinement mechanism is required. To accomplish that, the most often used structure is the so-called double channel planar buried heterostructure (DCPBH) [3] where a p-n-p-n structure on both sides of the narrow active region is introduced to block the current leakage

outside the active region. The fabrication of DCPBH structure requires a two-step liquid-phase epitaxy (LPE).

4.2 Processing of Multiple Section DFB Lasers

The processing of multiple section DFB stripe lasers is a non-routine procedure. Considerable effort had been dedicated to improve the processing technique where one of the main difficulties was to ensure proper impedance between neighboring sections (keep in mind that the middle section will be reverse biased). After time consuming trials and useful tips from T.R. Chen, the processing procedure had been finalized and is described as follows:

1. The wafer is cleaned in hot trichloroethylene (TCE) and subsequently rinsed in acetone, methanol, and de-ionized (DI) water.
2. A layer of silicon dioxide (silox) is grown on the wafer and by photolithography and etching in buffered hydrogen fluoride (HF), two symmetric $3\mu\text{m}$ openings (flanking the laser mesa) with $20\mu\text{m}$ separation are made on the silox.
3. Subsequently, the lateral electrical separations between neighboring sections are achieved by the etching of the $p^+ - \text{InGaAsP}$ and $p - \text{InP}$ layers in the $3\mu\text{m}$ openings in Br-methanol.
4. By photolithography and etching in the buffered HF, the $3\mu\text{m}$ openings on remaining silox in the perpendicular direction are formed using the specifically

designed mask SW102 (dark filled).

5. Next, the longitudinal electrical separations are implemented by etching of the $p^+ - InGaAsP$ layer in the newly opened $3\mu m$ windows.
6. The remaining silox is removed and the wafer is quickly (less than 5 seconds) dipped in 0.1% Br-methanol to smooth out the possible sharp edges from previous etchings.
7. A layer of silox is regrown on the wafer for the purpose of making stripe laser.
8. The $3\mu m$ (or $5/10\mu m$) openings on the silox is made *right* on top of the $1.5\mu m$ wide laser mesa by photolithography and etching in the buffered HF.
9. Using the photoresist pattern from last step to evaporate $250\text{ \AA}/500\text{ \AA}$ AuZn/Au by liftoff. So now the $3\mu m$ opening is filled with AuZn/Au.
10. $3\mu m$ separations (align with previous $3\mu m$ $p^+ - InGaAsP$ etch) on AuZn/Au is etched by using mask SW102 (dark filled).
11. The $150\text{ \AA}/1500\text{ \AA}$ Cr/Au p -contacts are evaporated by liftoff using mask SW102 (clear filled).
12. Subsequently, the p -contacts are annealed at $420^\circ C$ in hydrogen gas and the wafer is laped to approximately $3 \sim 4$ mils.
13. The $100\text{ \AA}/1500\text{ \AA}$ AuGe/Au n -contact is evaporated on the backside and then annealed at $380^\circ C$ in hydrogen gas.

14. Finally the wafer is cleaved, mounted, and if necessary wire bounded.

4.3 Experiment and Results

In this section, an experimental study of the three section semiconductor distributed-feedback lasers under the proposed pumping and biasing condition is presented [4]. The $1.3\mu\text{m}$ InGaAsP/InP semiconductor DFB lasers were grown by T.R. Chen in our group using liquid-phase epitaxy [5,6,7]. The wafers were then processed according to the procedures described in Section 4.2. The mounted lasers were then subjected to standard testing procedures to determine their quality.

First, the I-V characteristic between various p -contacts on the top side and the n -contacts on the back is measured. Here extreme care has to be taken to prevent subjecting the laser to excessive current. A good laser has typically very small current when the applied voltage is less than 0.7volts. Beyond 0.7volts, the current rises rapidly with slope is equal to or greater than 50mA/volt . A good practice is to increase the applied voltage very slowly and as soon as the rapid rise in current is observed the applied voltage should be withdrawn. It is best not to apply a voltage greater than 1.0volt. There is enough difference between 0.7volts and 1.0volt for one to determine the slope.

Next the electrical separations between section p -contacts are tested. Again one should be careful not to apply excessive current through the contacts.

Thirdly, the laser is checked for lasing using current pulses (typically 100ns with

a 50kHz repetition rate). The L-I (light power versus current) curve is plotted from which the threshold current and the quantum efficiency can be determined. The quantum efficiency is given by

$$\eta = \frac{e}{E_g} \frac{dL}{dI} \quad (4.1)$$

where e is the electric charge of an electron and E_g is the bandgap energy of the active layer (InGaAsP).

Finally, the laser is tested for CW operation. After that the laser is ready for measurements of linewidth and modulation response. A current supply with a suitable current limiting mechanism is advised.

The experimental methods employed for linewidth measurement were the delayed-self-heterodyne and scanning Fabry-Perot. The system setup is shown in Figure 4.1 where the laser output is split into two beams: One is directed to a scanning FP setup and the other to a delayed-self-heterodyne. The acoustooptic (AO) crystal is driven by an RF signal at 150MHz. The output from the AO crystal is comprised of two laser beams, one at the original frequency and one at a shifted frequency (by 150MHz, the RF frequency) [8]. The two beams are then combined at a square law detector after one beam is properly delayed using a long fiber. The output from the detector is then directed to an RF spectrum analyzer.

The single mode operation was checked and its wavelength was measured using an optical spectrum analyzer. The laser beam was coupled into a single-mode fiber and directed to an HP TQ8346 optical spectrum analyzer. The result for one of the lasers (SW-2-10) tested is shown in Figure 4.2 which clearly shows a single mode laser

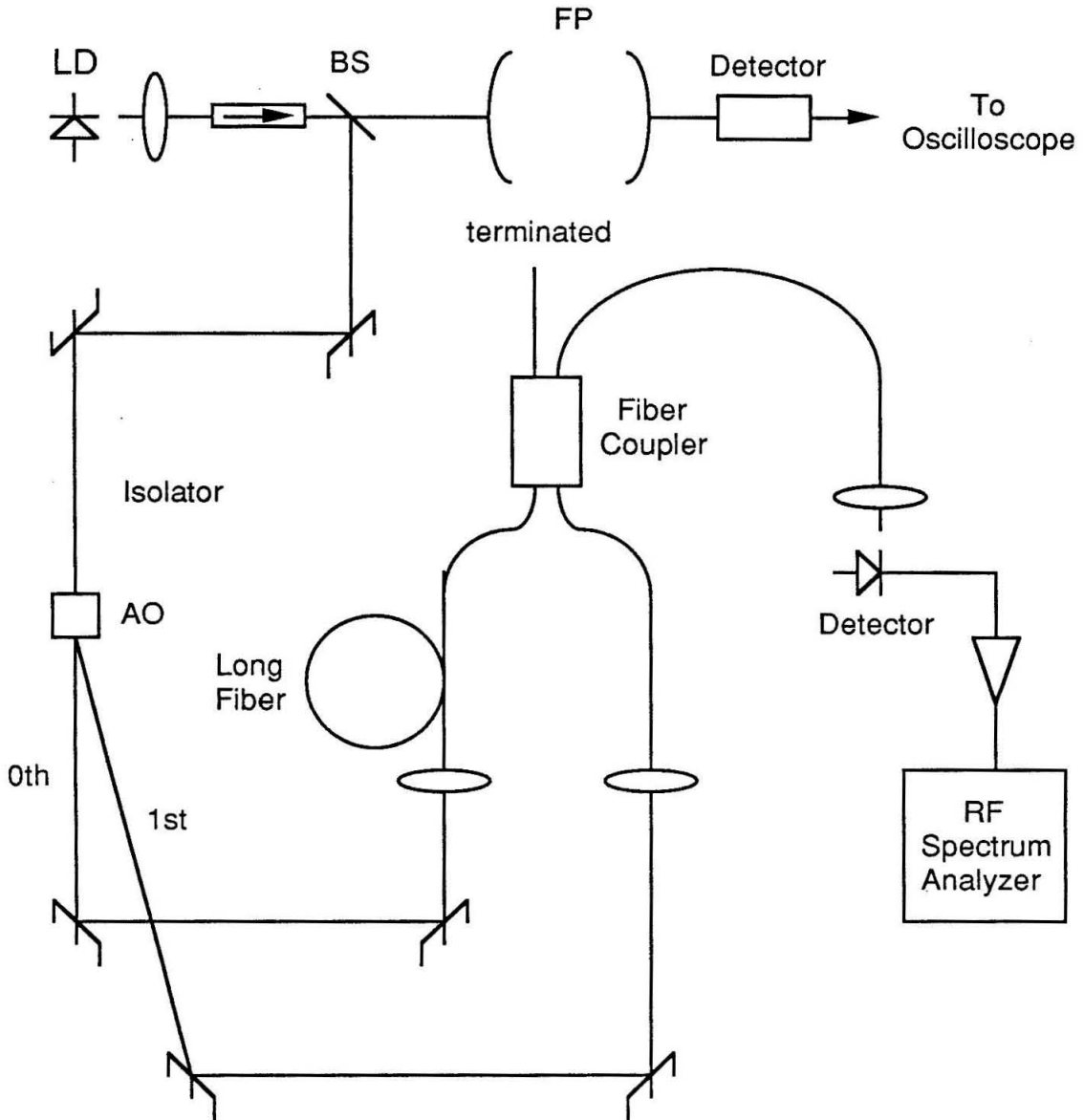


Figure 4.1: Experimental setup for laser linewidth measurements by a scanning Fabry-Perot etalon and the delayed-self-heterodyne technique. The laser beam is incident upon the AO, an acousto-optic crystal driven by an RF signal at 150MHz. The output is comprised of two beams, the zeroth order and the first order, propagating in different directions. The zeroth and first order beams are at the original optical frequency ω and a shifted frequency $\omega + 150MHz$, respectively.

operation with lasing wavelength

$$\lambda = 1.30567\mu m$$

The result of laser linewidth measurements under different pumping and biasing conditions follows. On the SW-2-10 laser a linewidth reduction of a factor of 20 was observed (see Figure 4.3). The SW-2-10 laser has a threshold current of 86mA. Its first end, middle, and second end sections have lengths of $450\mu m$, $50\mu m$, and $300\mu m$, respectively. When only the first cavity (lasing section) was pumped well above threshold (120.2mA) with the second cavity unpumped and middle section unbiased or all three sections were pumped uniformly, the laser had a linewidth of 60MHz at approximately 4mW output power. When the middle section was reverse biased (-0.3 volts) and the pumping current of the second cavity was gradually increased, it is observed that, with the pumping current for the first section fixed at 120.2mA, the output power did not change more than $\pm 15\%$ while at $I_2 = 87.8$ mA the laser linewidth was 3MHz. The lineshape was verified to be of a Lorentzian. The same reduction was observed also with laser SW-2-9.

On a different group of lasers, a free running first end section of 4MHz linewidth at approximately 3mW output power was observed. When the proposed pumping and biasing was carried out the linewidth was reduced to 1MHz again with output power changed less than 10% (the observed power actually decreased during linewidth narrowing), which is shown in Figure 4.4. This was observed on every good laser from the group (about 75% of them were good). On one laser, a linewidth of approximately

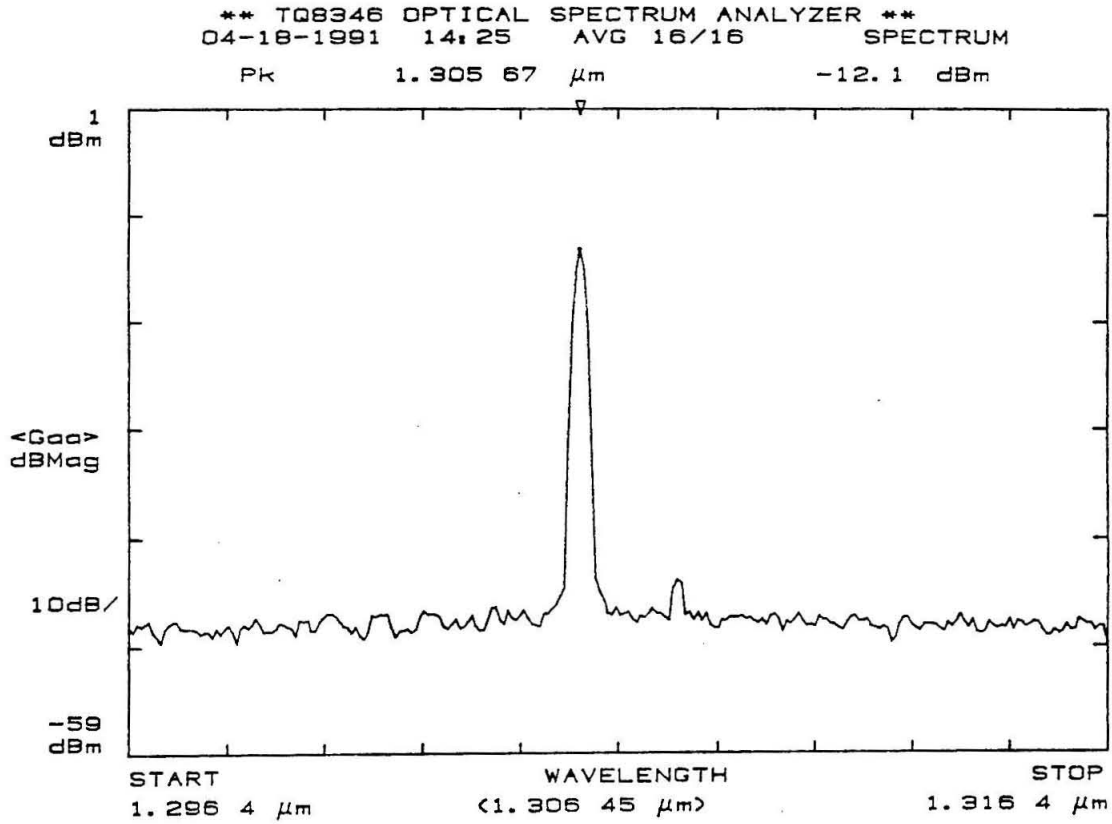


Figure 4.2: Measured optical spectrum of a DFB laser. It shows clearly a single mode operation at $1.30567\mu\text{m}$ wavelength.

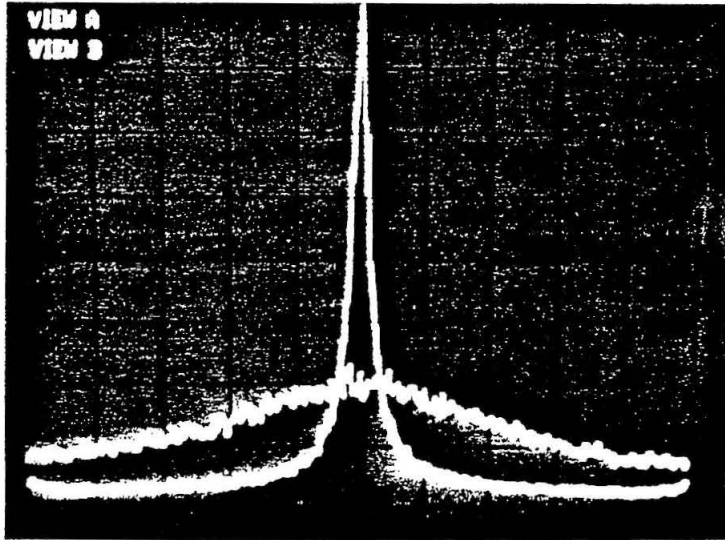


Figure 4.3: Experimental observation of laser linewidth reduction (#1). The horizontal scale is 20MHz/division and the vertical axis is on linear scale. The broader spectrum with 60MHz linewidth was observed when only the first end section was pumped. The narrower lineshape with 3MHz linewidth was observed when the proposed pumping and biasing condition was used. Under both pumping scenarios, the laser output power was approximately 4mW.

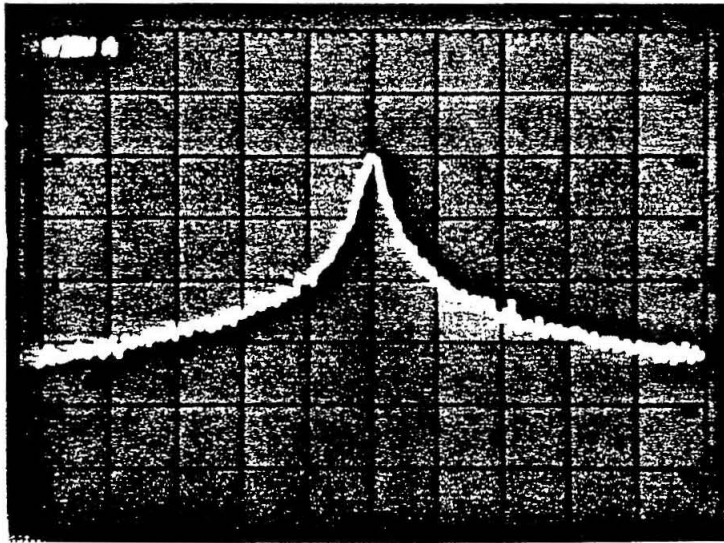
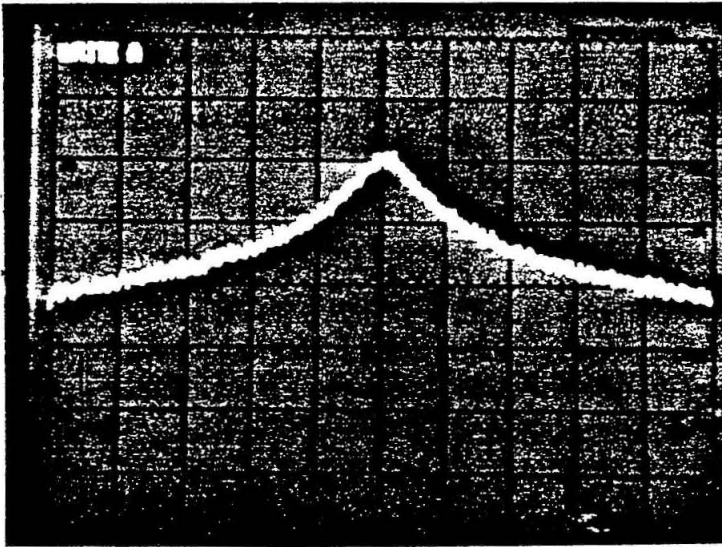


Figure 4.4: Experimental observation of laser linewidth reduction (#2). The horizontal and vertical scales are 10MHz/division and 10dB/division, respectively. The broader spectrum with 4MHz linewidth was observed when only the first end section was pumped. The narrower lineshape with 1MHz linewidth was observed when the proposed pumping and biasing condition was used. Under both pumping scenarios, the laser output power was approximately 3mW.

300kHz at 3mW output power was observed under the proposed pumping and biasing condition for about three minutes. This very narrow linewidth was a one time occurrence and could not be repeated.

4.4 Discussions

It has been demonstrated experimentally that a moderate reduction in laser linewidth can be achieved. The theoretical prediction of a reduction of $10 \sim 20$ was observed experimentally. As anticipated in the theoretical prediction, the reduction of linewidth by 100 or more is possible but requires mode matching between the two cavities. This section is devoted to discussions of possible improvements in terms of obtaining even narrower laser linewidths.

The mode matching simply means that the lasing wavelength of the first cavity matches that of the second cavity. In DFB lasers the lasing frequency is given by [5]

$$\omega_m = \omega_0 - \left(m + \frac{1}{2}\right) \frac{\pi c}{n_{eff} L} \quad (4.2)$$

where

$$\omega_0 = \frac{l\pi c}{n_{eff}\Lambda}$$

and Λ is grating period, m and l are integers, and L is cavity length. The mode spacing (in frequency) is

$$\frac{\pi c}{n_{eff} L}$$

which is about 8 \AA in wavelength spacing for $L = 300\mu m$. If both end sections lase at the same mode m (which is very likely), for example $m = 0$, then the difference

in lasing wavelength is due to different pumping current and cavity lengths. In this case, the mode matching can be achieved by pumping current adjustment which has a greater observed tuning range (4 \AA) than the wavelength difference (2 \AA) due to different cavity lengths.

If the lasing section is wavelength tunable, then one more adjustable control with greater tunability over the laser is available and, hence, the mode matching becomes easier to achieve. Therefore, by converting the first section into a two (or three) section (possibly phase shifted) inhomogeneously pumped laser would ensure the achievement of mode matching.

The use of DFB quantum well laser in lieu of a heterostructure DFB in the proposed scheme would likely result in further narrowing of linewidth as well as improved tunability.

To conclude this chapter, a moderate reduction in laser linewidth was demonstrated by employing three section $1.3\mu\text{m}$ InGaAsP/InP heterostructure DFB lasers and the pumping and biasing scheme proposed in Chapter 3. The linewidth reduction scheme as proposed has the potential to result in reductions well beyond those which were theoretically predicted and experimentally observed in this work. Finally, the proposed scheme is thus far (to the best of author's knowledge) the only monolithic method for possibly achieving the magnitude of reduction observed in external feedback scenarios.

4.5 References

- [1] M. Nakamura, A. Yariv, H. W. Yen, S. Somekh, and H. L. Garvin, *Appl. Phys. Lett.*, **22**, 515(1973).
- [2] M. Nakamura, W. H. Yen, A. Yariv, E. Garmire, S. Somekh, and H. L. Garvin, *Appl. Phys. Lett.*, **23**, 224(1973).
- [3] I. Mito, et al., *IEEE J. Lightwave Tech.* **LT-1**, 195(1983).
- [4] S. Wu, Y. Shevy, T. R. Chen, and A. Yariv, "Observation of linewidth reduction in three section distributed-feedback lasers," in preparation.
- [5] A. Yariv, *Quantum Electronics*, 3rd ed. (John Wiley & Sons, New York, 1989).
- [6] H. C. Casey and M. B. Panish, *Heterostructure Lasers*, (Academic Press, New York, 1978).
- [7] R. D. Dupuis and P. D. Dapkus, *Appl. Phys. Lett.*, **31**, 466(1977).
- [8] A. Yariv and P. Yeh, *Light Propagation in Crystals*, (John Wiley & Sons, New York, 1980).

Chapter 5

Rayleigh Scattering Induced Phase-to-Intensity Noises in Optical Fibers

5.1 An Introduction

From Section 2.4, we know that at the output of a semiconductor laser, the electric field typically has negligible amplitude fluctuations but significant phase fluctuations due to spontaneous emission [1,2,3]. As a result, if the laser light is incident directly upon a “square law” detector then the detected photocurrent has negligible fluctuations because square law detection is insensitive to the phase. If the laser light is split into two or more beams and which are combined at a square law detector with nonzero relative time delay, generally the detected light intensity of the interfering beams will

be temporally modulated and consequently an intensity fluctuation results. This is known as phase-to-intensity conversion noise.

Rayleigh scattering is generally defined as scattering of waves due to inhomogeneity on a scale that is smaller than that of the wavelength. In optical fibers, because of the thermodynamically frozen inhomogeneities, the propagating beam undergoes Rayleigh scattering. Due to the waveguide nature of optical fibers, only a special form of Rayleigh scattering, specifically Rayleigh backscattering into the propagating mode matters. Of course there exist transitions from a confined to radiative modes due to Rayleigh scattering in optical fibers, however, that portion of Rayleigh scattering is not of interest in this work and will be included as a part of optical losses characterized by the loss coefficient α [7,8].

Because of the Rayleigh backscattering, the laser light at the output of a long optical fiber contains not only the direct transmitted beam but also Rayleigh double backscattered beams. The resulting interference converts the inherent phase fluctuations due to spontaneous emission in the output of the laser to intensity fluctuations at the output end of the fiber [4,5,6,9]. These fluctuations have emerged as limits to performance in some critical long distance fiber applications. Due to the nature of fiber inhomogeneities, the amplitude and occurrence of Rayleigh scattering are random. Current work [10,11,12,13,14] deals with the coherent nature of the problem, however, a full statistical theory taking into account both random phase fluctuations and fiber inhomogeneities has not been developed. It, thus, became necessary to develop a fundamental theory which will enable us to determine the intensity noise level

due to this phenomenon in a wide variety of cases. To this end, the laser Langevin-oscillator equation for the phase statistics of the laser field was solved and the result is applied to a statistical noise analysis of the scattering problem in the fiber in the context of simple wave mixing. The result is a set of expressions for the total scattered power under a variety of experimental configurations as well as for the spectrum of the resulting intensity fluctuations. The theoretical predictions and their practical implications will be compared in Chapter 6 with experiments employing fiber lengths of up to 20km and semiconductor laser sources.

5.2 Statistics of Semiconductor Laser Noise and Index Fluctuations in Optical Fibers

In this section the mathematical tools are developed and the necessary background is introduced for developing a statistical theory describing the phenomenon of phase-to-intensity conversion noise in optical fibers. Some of the basic mathematical results which will be used repeatedly in the next section are also included.

The electric field at the output of a semiconductor laser is of the form

$$E(t) = E_0 e^{i[\omega t + \phi(t)]} \quad (5.1)$$

where ω is the lasing frequency, $\phi(t)$ is the random phase due to the spontaneous emission, and E_0 is the amplitude (whose fluctuations are neglected). A statistical analysis (see Section 2.3) of the phase fluctuation using a Van-der-Pol oscillator model

driven by Langevin noise source leads to [1,3]

$$\langle \Delta\phi(\tau_1)\Delta\phi(\tau_2) \rangle = \frac{2}{\tau_c} \min(\tau_1, \tau_2) \quad (5.2)$$

where $\Delta\phi(\tau) \equiv \phi(t + \tau) - \phi(t)$, $\tau_1, \tau_2 \geq 0$ and τ_c is the coherence time of the laser.

In developing a statistical theory of phase-to-intensity conversion noise in optical fibers, it is necessary to know the correlation function

$$\langle \Delta\phi(\tau_1)\Delta\phi(\tau_2) \rangle$$

for arbitrary τ_1 , and τ_2 that take both positive and negative values. Let us consider two special cases and then deduce a general conclusion.

1. For $0 \geq \tau_2 \geq \tau_1$

$$\Delta\phi(\tau_1) = \phi(t + \tau_1) - \phi(t) = -[\phi(t' - \tau_1) - \phi(t')]$$

where $t' \equiv t + \tau_1$. Define

$$\Delta'\phi(\tau) \equiv \phi(t' + \tau) - \phi(t')$$

we have

$$\Delta\phi(\tau_1) = -\Delta'\phi(-\tau_1)$$

$$\Delta\phi(\tau_2) = \Delta'\phi(\tau_2 - \tau_1) - \Delta'\phi(-\tau_1)$$

$$\begin{aligned} \langle \Delta\phi(\tau_1)\Delta\phi(\tau_2) \rangle &= \langle -\Delta'\phi(-\tau_1)[\Delta'\phi(\tau_2 - \tau_1) - \Delta'\phi(-\tau_1)] \rangle \\ &= \frac{2}{\tau_c} [-(\tau_2 - \tau_1) + (-\tau_1)] \\ &= -\frac{2}{\tau_c} \tau_2 \\ &= \frac{2}{\tau_c} \min(|\tau_1|, |\tau_2|) \end{aligned}$$

2. Similarly for $\tau_1 \leq 0, \tau_2 \geq 0$, we have

$$\begin{aligned}
\Delta\phi(\tau_1) &= -\Delta'\phi(-\tau_1) \\
\Delta\phi(\tau_2) &= \Delta'\phi(\tau_2 - \tau_1) - \Delta'\phi(-\tau_1) \\
\langle \Delta\phi(\tau_1)\Delta\phi(\tau_2) \rangle &= \langle -\Delta'\phi(-\tau_1)[\Delta'\phi(\tau_2 - \tau_1) - \Delta'\phi(-\tau_1)] \rangle \\
&= \frac{2}{\tau_c}[-(-\tau_1) + (-\tau_1)] \\
&= 0
\end{aligned}$$

In conclusion, the second order correlation function is given by

$$\langle \Delta\phi(\tau_1)\Delta\phi(\tau_2) \rangle = \begin{cases} \frac{2}{\tau_c} \min(|\tau_1|, |\tau_2|) & \text{if } \tau_1\tau_2 \geq 0 \\ 0 & \text{if } \tau_1\tau_2 < 0 \end{cases} \quad (5.3)$$

The optical field linewidth is a result of the random phase fluctuations and can be determined using Equation 5.3, as follows

$$\begin{aligned}
C_E(\tau) &= \langle E(t)E(t + \tau) \rangle \\
&= \frac{E_0^2}{2} \Re \langle e^{i\omega\tau} e^{i\Delta\phi(\tau)} \rangle \\
&= \frac{E_0^2}{2} e^{-\tau/\tau_c} \cos \omega\tau \quad (5.4)
\end{aligned}$$

$$\begin{aligned}
W_E(\Omega) &= \frac{2}{\pi} \int_0^\infty C_E(\tau) \cos \Omega\tau d\tau \\
&= \frac{E_0^2}{2} \frac{\tau_c/\pi}{1 + (\Omega - \omega)^2 \tau_c^2} \quad \text{for } \Omega \approx \omega \quad (5.5)
\end{aligned}$$

$$\Delta\nu_{laser} = \frac{1}{\pi\tau_c} \quad (5.6)$$

where $C_E(\tau)$ is the correlation function of the electric field, $W_E(\Omega)$ is the spectral density function of optical field, $\Delta\nu_{laser}$ is the laser linewidth (full width at half

maximum or FWHM), and

$$\langle e^{i\Delta\phi(\tau)} \rangle = e^{-\tau/\tau_c}$$

by using Equation 5.3 and Wick's theorem (see Appendix A).

The linewidth can be measured by employing the delayed-self-homodyne method with a long fiber delay such that the delay time is much greater than the coherence time τ_c of the laser. The resulting spectral density function in case of an arbitrary time delay is derived in Appendix B and Reference [6].

Rayleigh scattering in optical fibers is due to the random density inhomogeneities which are thermodynamically frozen during the manufacturing process. As a result, all optical fibers have a nonuniform distribution of index of refraction whose statistics are completely described by the correlation relationship

$$\langle \Delta n(z)\Delta n(z') \rangle = \beta^2 e^{-|z-z'|/z_R} \quad (5.7)$$

where $\Delta n(z) = n(z) - n_0$, $n(z)$ is the index of refraction at z , n_0 is the average index of refraction in the fiber, $\langle \Delta n^2(z) \rangle = \beta^2$, and z_R is the coherence length. In the next section we model a single-mode fiber as made up of infinite number of equal length sections with length $a \rightarrow 0$. Thus, Equation 5.7 can be rewritten as

$$\langle \Delta n_j \Delta n_{j'} \rangle = \beta^2 e^{-|j-j'|a/z_R} \quad (5.8)$$

where $z = ja$, $z' = j'a$, and j, j' are integers. One of the correlations that will occur in the next section is evaluated as

$$\langle (\Delta n_{j+1} - \Delta n_j)(\Delta n_{l+1} - \Delta n_l) \rangle = \frac{2a\beta^2}{z_R} (\delta_{jl} - \frac{a}{2z_R} e^{-|j-l|a/z_R}) \quad (5.9)$$

The fourth order correlation functions which will be encountered in the next section can be readily evaluated using Wick's theorem. In Appendix A, the theorem is stated and its proper application is demonstrated in an example.

5.3 Theory of Phase-to-Intensity Conversion Noise due to Rayleigh Scattering in Optical Fibers

From knowledge of the laser phase fluctuation statistics and that of the fiber spatial inhomogeneities, the intensity noise of the detected photocurrent due to Rayleigh scattering in optical fibers can be derived [6]. Consider three generic cases:

1. Double Rayleigh scattering that involves the beating of the unscattered (direct) beam with light which arrives at the far (receiving) end of the fiber following two Rayleigh scattering events (see Figure 5.1).
2. Beating between the direct light and the (once) Rayleigh scattered light which is redirected toward the output end of the fiber by a fixed reflection at the input side (see Figure 5.2).
3. The simple case of Rayleigh scattered light emerging from the input end (see Figure 5.3).

In each of these cases the intensity at the output of the fiber contains an interference term between light components which left the laser at different times. Since the

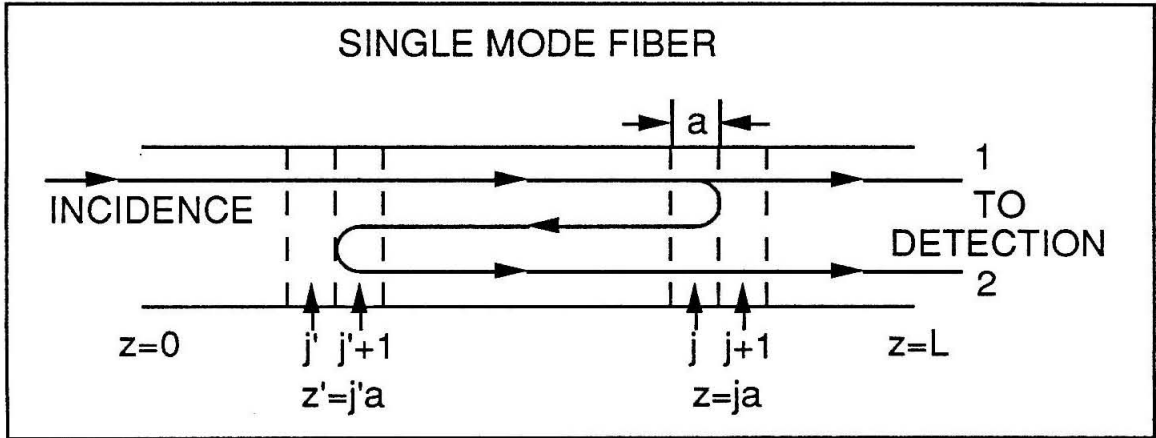


Figure 5.1: Double Rayleigh scattering in optical fibers. A single-mode fiber is modeled as made up of $N(\rightarrow \infty)$ sections, of length $a = L/N(\rightarrow 0)$, with effective indices of refraction n_1, n_2, \dots, n_N . Beam 1 and 2 are direct transmitted and twice Rayleigh backscattered (first at $z = ja$, then at $z' = j'a$, where $0 \leq z' < z \leq L$) light, respectively. The total field at $z = L$ is the sum of that of beam 1 and 2.

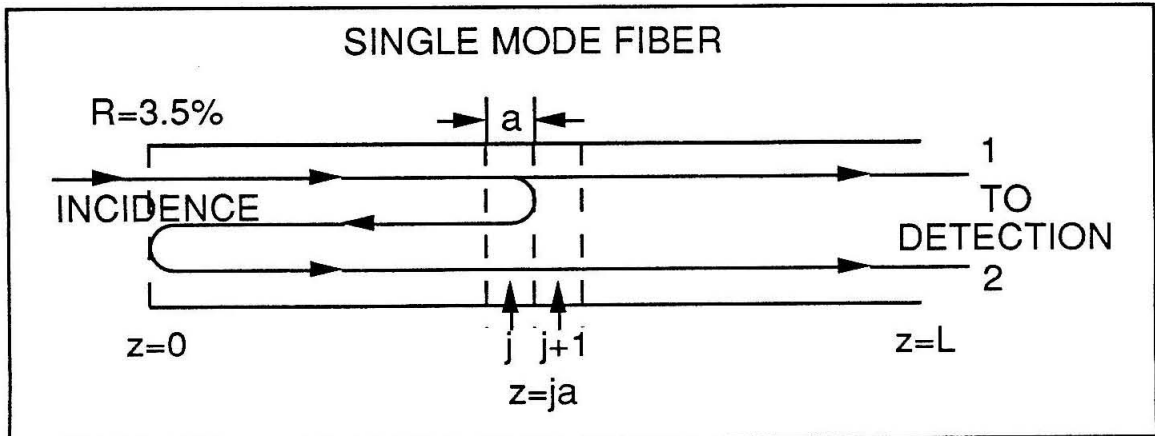


Figure 5.2: Redirected Rayleigh scattering in optical fibers. Beam 1 and 2 are direct transmitted and (once) Rayleigh scattered (at $z = ja$, where $0 < z \leq L$) light which then is redirected (at $z = 0$, due to fiber-air interface,) toward the output end of the fiber, respectively. The total field at $z = L$ is the sum of that of beam 1 and 2.

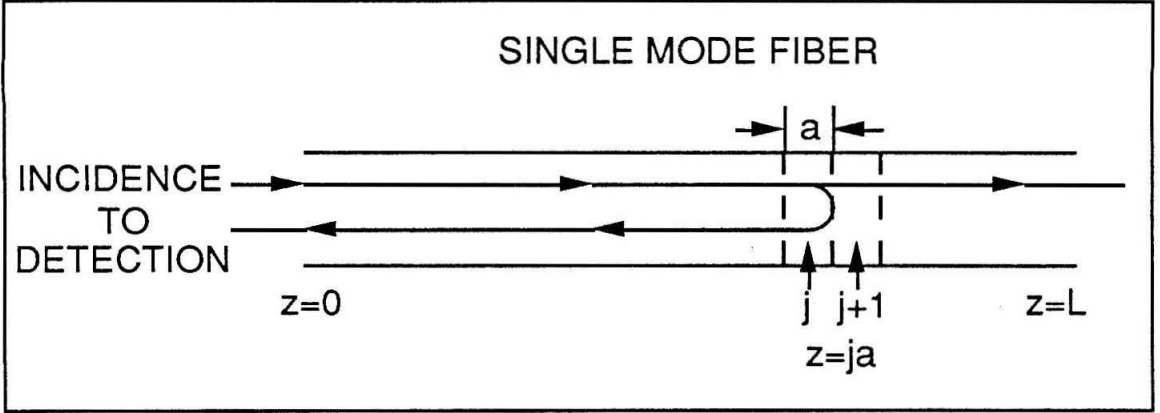


Figure 5.3: Rayleigh backscattering in optical fibers. The laser light is Rayleigh backscattered at $z = ja$, where $0 < z \leq L$.

laser phase fluctuates randomly, the total transmitted light intensity is temporally modulated.

Double Rayleigh scattering in optical fibers

We start with double Rayleigh scattering. The single mode fiber is modeled as made up of N ($\rightarrow \infty$) sections with effective indices of refraction n_1, n_2, \dots, n_N (see Figure 5.1). The total field at the detector is the sum of the “direct” beam and the doubly scattered beam

$$E_T(L, t) = E_0 e^{i[\omega t + \phi(t)]} e^{-\alpha L/2} \left\{ 1 - \frac{1}{4n_0^2} \sum_{j=1}^{L/a} \sum_{j'=0}^{j-1} (\Delta n_{j+1} - \Delta n_j)(\Delta n_{j'+1} - \Delta n_{j'}) \right. \\ \left. \cdot e^{-(\alpha + 2ik)(j-j')a} e^{i\left\{\phi\left[t - \frac{2(j-j')a}{v}\right] - \phi(t)\right\}} \right\} \quad (5.10)$$

where α is the loss coefficient, L is the fiber length, $a = L/N$ ($\rightarrow 0$), k is the propagation constant of laser light in the fiber, v is the group velocity, and the Rayleigh

backscattering coefficient at $z = ja$ is

$$\frac{\Delta n_j - \Delta n_{j+1}}{2n_0}$$

Although it is not expressly indicated, the limit $a = L/N \rightarrow 0$ is understood throughout this section. The photocurrent $I(t)$ is taken as

$$I(t) \propto \frac{1}{2} s_d |E_T(L, t)|^2 \quad (5.11)$$

$$I(t) = s_d I_0 e^{-\alpha L} \left\{ 1 - \left[\frac{1}{4n_0^2} \sum_{j=1}^{L/a} \sum_{j'=0}^{j-1} (\Delta n_{j+1} - \Delta n_j) (\Delta n_{j'+1} - \Delta n_{j'}) \right. \right. \\ \left. \left. \cdot e^{-(\alpha+2ik)(j-j')a} e^{i\{\phi[t-\frac{2(j-j')a}{v}]-\phi(t)\}} + c.c. \right] \right\} \quad (5.12)$$

where we have neglected the terms due to the beating of the scattered light with itself which are fourth order in $\Delta n(z)$, s_d is responsivity of the detector (*photocurrent* = $s_d \times \text{power}$), and I_0 is the incident power.

The autocorrelation function of the photocurrent is defined as

$$C(\tau) \equiv \langle I(t)I(t+\tau) \rangle_{t,e} \quad (5.13)$$

where the subscript t and e indicate the time average for the temporal part and the ensemble average for the index fluctuations, respectively. Using Equation 5.12, we obtain

$$C(\tau) = s_d^2 I_0^2 e^{-2\alpha L} \left\{ 1 + \frac{1}{8n_0^4} \Re \left\{ \sum_{j=1}^{L/a} \sum_{j'=0}^{j-1} \sum_{l=1}^{L/a} \sum_{l'=0}^{l-1} \langle (\Delta n_{j+1} - \Delta n_j) (\Delta n_{j'+1} - \Delta n_{j'}) \right. \right. \\ \cdot (\Delta n_{l+1} - \Delta n_l) (\Delta n_{l'+1} - \Delta n_{l'}) \rangle_e e^{-\alpha(j-j'+l-l')a} e^{-2ik(j-j')a} \\ \cdot [e^{-2ik(l-l')a} \langle e^{i\{\phi[t-\frac{2(j-j')a}{v}]-\phi(t)+\phi[t+\tau-\frac{2(l-l')a}{v}]-\phi(t+\tau)\}} \rangle_t \\ \left. \left. + e^{2ik(l-l')a} \langle e^{i\{\phi[t-\frac{2(j-j')a}{v}]-\phi(t)-\phi[t+\tau-\frac{2(l-l')a}{v}]+\phi(t+\tau)\}} \rangle_t \right] \right\} \quad (5.14)$$

Using the Wick's theorem (see Appendix A), the fourth order correlation functions encountered in Equation 5.14 are evaluated as

$$\langle e^{i\{\phi[t-\frac{2(j-j')a}{v}]-\phi(t)+\phi[t+\tau-\frac{2(l-l')a}{v}]-\phi(t+\tau)\}} \rangle_t = e^{-\frac{1}{\tau_c}[|\tau+\frac{2(j-j')a}{v}|+|\tau-\frac{2(l-l')a}{v}|]} \quad (5.15)$$

$$\langle e^{i\{\phi[t-\frac{2(j-j')a}{v}]-\phi(t)-\phi[t+\tau-\frac{2(l-l')a}{v}]+\phi(t+\tau)\}} \rangle_t = e^{-\frac{1}{\tau_c}[|\tau|+|\tau-\frac{2(l-l')a}{v}|+|\frac{2(j-j')a}{v}|]} \quad (5.16)$$

It is a straightforward, but tedious, exercise to carry out the quadruple integrations and finally obtain

$$C(\tau) = s_d^2 I_0^2 e^{-2\alpha L} \left\{ 1 + 4(\alpha L_{eff}) \left(\frac{\beta^2 k^2 z_R}{n_0^2 \alpha} \right)^2 e^{-2\tau/\tau_c} \right\} \quad (5.17)$$

where

$$L_{eff} = L - \frac{1}{2\alpha}(1 - e^{-2\alpha L}) \quad (5.18)$$

The spectral density function $W_I(\Omega)$ of the detected photocurrent at frequency Ω is obtained using the Wiener-Khintchine theorem [3]

$$W(\Omega) = \frac{2}{\pi} \int_0^\infty C(\tau) \cos \Omega \tau d\tau \quad (5.19)$$

and is evaluated using Equation 5.17

$$W_I(\Omega) = s_d^2 I_0^2 e^{-2\alpha L} \left\{ 2\delta(\Omega) + \frac{4}{\pi} (\alpha L_{eff}) \left(\frac{\beta^2 k^2 z_R}{n_0^2 \alpha} \right)^2 \frac{\tau_c}{1 + (\frac{1}{2}\Omega\tau_c)^2} \right\} \quad (5.20)$$

We use the conventional definition of the relative intensity noise (RIN) of a laser at an RF frequency Ω as the ratio of the photocurrent fluctuation “power” (in $\Delta\Omega = 1Hz$) to the average power. From Equation 5.20 the RIN is given by

$$RIN = 4(\alpha L_{eff}) \left(\frac{\beta^2 k^2 z_R}{n_0^2 \alpha} \right)^2 \frac{\tau_c}{1 + (\frac{1}{2}\Omega\tau_c)^2} \quad (5.21)$$

Redirected Rayleigh scattering in optical fibers

In the case of the redirected Rayleigh scattering (see Figure 5.2), we obtain

$$E_T(L, t) = E_0 e^{i[\omega t + \phi(t)]} e^{-\alpha L/2} \left\{ 1 - \frac{r}{2n_0} \sum_{j=1}^{L/a} (\Delta n_{j+1} - \Delta n_j) \right. \\ \left. \cdot e^{-(\alpha + 2ik)ja} e^{i[\phi(t - \frac{2ja}{v}) - \phi(t)]} \right\} \quad (5.22)$$

$$I(t) = s_d I_0 e^{-\alpha L} \left\{ 1 - \frac{r}{2n_0} \Re \left\{ \sum_{j=1}^{L/a} (\Delta n_{j+1} - \Delta n_j) \right. \right. \\ \left. \left. \cdot e^{-(\alpha + 2ik)ja} e^{i[\phi(t - \frac{2ja}{v}) - \phi(t)]} \right\} \right\} \quad (5.23)$$

where we have neglected the terms that are of order $r^2(\Delta n)^2$, $R = r^2$ is the reflection coefficient at the fiber input end, and

$$W_I(\Omega) = s_d^2 I_0^2 e^{-2\alpha L} \left\{ 2\delta(\Omega) + \frac{2R}{\pi} \left(\frac{\alpha}{\alpha_{eff}} \right) \left(\frac{\beta^2 k^2 z_R}{n_0^2 \alpha} \right) \frac{\tau_c}{1 + (\frac{1}{2}\Omega\tau_c)^2} \right\} \quad (5.24)$$

$$RIN = 2R \left(\frac{\alpha}{\alpha_{eff}} \right) \left(\frac{\beta^2 k^2 z_R}{n_0^2 \alpha} \right) \frac{\tau_c}{1 + (\frac{1}{2}\Omega\tau_c)^2} \quad (5.25)$$

where

$$\frac{1}{\alpha_{eff}} = \frac{1}{\alpha} (1 - e^{-2\alpha L}) \quad (5.26)$$

Rayleigh backscattering in optical fibers

Similarly, in the case of simple Rayleigh backscattering (see Figure 5.3), we have

$$E_R(0, t) = - \sum_{j=1}^{L/a} \frac{\Delta n_{j+1} - \Delta n_j}{2n_0} E_0 e^{i[\omega t - 2kja + \phi(t - \frac{2ja}{v})]} \quad (5.27)$$

$$I(t) = \frac{s_d I_0}{4n_0^2} \Re \left\{ \sum_{j=1}^{L/a} \sum_{j'=1}^{L/a} (\Delta n_{j+1} - \Delta n_j) (\Delta n_{j'+1} - \Delta n_{j'}) e^{-\alpha(j+j')a} \right. \\ \left. \cdot e^{-2ik(j-j')a} e^{i[\phi(t - \frac{2ja}{v}) - \phi(t - \frac{2j'a}{v})]} \right\} \quad (5.28)$$

$$W_I(\Omega) = s_d^2 I_0^2 \left(\frac{\beta^2 k^2 z_R}{n_0^2 \alpha} \right)^2 \left(\frac{\alpha}{\alpha_{eff}} \right)^2 \left\{ 2\delta(\Omega) + \frac{1}{\pi} \frac{\tau_c}{1 + \left(\frac{1}{2} \Omega \tau_c \right)^2} \right\} \quad (5.29)$$

$$RIN = \frac{\tau_c}{1 + \left(\frac{1}{2} \Omega \tau_c \right)^2} \quad (5.30)$$

From integration of the first term in the curly brackets in Equation 5.29 over all Ω it follows that the fraction of incident power which is reflected into the fiber guided mode by Rayleigh backscattering is

$$\frac{\beta^2 k^2 z_R}{n_0^2 \alpha_{eff}}$$

A comparison of the three spectra Equations 5.20, 5.24, and 5.29 shows that the frequency dependence in each case is identical, specifically, a *Lorentzian* lineshape [3] with a width $4/\tau_c$ which is twice that of the laser optical field spectrum. The scattering strength of the fiber is represented in all three cases by the parameter S_R defined as

$$S_R \equiv \frac{\beta^2 k^2 z_R}{n_0^2 \alpha} \quad (5.31)$$

This parameter is also equal, according to Equations 5.26 and 5.29, to the fraction of laser power which is reflected in a very long ($L \gg \frac{1}{\alpha}$) fiber.

In summary, the basic statistical fluctuations of optical fiber inhomogeneities and of the quantum phase of the laser field have been used to derive the spectra of the detected photocurrent in a number of generic cases involving the ubiquitous Rayleigh scattering which are important to optical fiber communication systems. The results show that the noise spectra have Lorentzian lineshapes whose magnitude depends on a single parameter measuring the scale of index fluctuations in optical fibers.

5.4 References

- [1] K. Vahala and A. Yariv, *IEEE J. of Quant. Elec.*, **QE-19**, 1096(1983).
- [2] K. Vahala and A. Yariv, *IEEE J. of Quant. Elec.*, **QE-19**, 1102(1983).
- [3] A. Yariv, *Quantum Electronics*, 3rd ed. (John Wiley & Sons, New York, 1989).
- [4] P. Gysel and R. K. Staubli, *IEEE Photon. Tech. Lett.*, **1**, 327(1989).
- [5] S. Wu, A. Yariv, H. Blauvelt, and N. Kwong, *Appl. Phys. Lett.*, **59**, 1156(1991).
- [6] S. Wu, A. Yariv, H. Blauvelt, and N. Kwong, "A theoretical study of phase-to-intensity conversion noise by Rayleigh scattering in optical fiber links," to be published.
- [7] T. Miya, Y. Terunuma, T. Hosaka, and T. Miyashita, *Electron. Lett.*, **15**, 106(1979).
- [8] M. K. Barnoski and S. M. Jensen, *Appl. Opt.*, **20**, 1060(1976).
- [9] A. F. Judy, presented at the *European Conference on Optical Communication*, Gteborg, Sweden, 1989, paper TuP-11.
- [10] E. Brinkmeyer, *Electron. Lett.*, **16**, 329(1980).
- [11] M. Nakazawa, *IEEE J. Quant. Elec.*, **QE-19**, 854(1983).
- [12] W. Eickhoff and R. Ulrich, *Appl. Phys. Lett.*, **39**, 693(1981).
- [13] H. Ghafoori-Shiraz and T. Okoshi, *Opt. and Qunat. Tech.*, **18**, 265(1986).

- [14] J. Mark, Ph.D. thesis, Electromagnetics Institute, Technical University of Denmark, Lyngby, Denmark.
- [15] A. Yariv, *Opt. Lett.*, **15**, 1064(1990).
- [16] R. J. Mears, L. Reekie, I. M. Jauncey, and D. N. Payne, *Electron. Lett.*, **23**, 1026(1987).

Chapter 6

Experimental Study of Rayleigh

Scattering Induced Intensity

Noise in Optical Fibers

6.1 An Introduction

In Chapter 5, a statistical theory for conversion of phase fluctuation (in the output of a semiconductor laser) to intensity fluctuation (at the output of a long haul fiber link) due to Rayleigh scattering in optical fibers was developed. The results are a set of simple equations predicting the intensity spectra and relative intensity noise (RIN) in various generic cases. The numerical predictions can be readily obtained for different cases if the coherence time of laser and the single physical parameter S_R (see Equation 5.31) are known.

In this chapter the experimental study of Rayleigh scattering induced phase-to-intensity noise in three generic cases with different fiber lengths is presented [1]. Several methods can be used to measure the optical linewidth of a laser. The most often used are: The scanning Fabry-Perot etalon [2], the delayed-self-homodyne measurement technique [3,4], and the delayed-self-heterodyne method. In addition Rayleigh scattering in optical fibers itself can be used for measuring laser linewidths which will be shown later in this chapter. In the experiment the delayed-self-homodyne method was used to measure laser linewidth and, hence, the coherence time. The experiment was set up to simulate the three generic cases described in Section 5.3. In each case, the relative intensity noise (RIN) was measured for varying fiber length. One of the measured RIN data was used to determine the parameter S_R . Then the numerical predictions were calculated using the equations from Section 5.3 and comparison with the measurements was conducted.

6.2 Measurement of the Coherence Time

One experimental method to obtain the optical linewidth of laser is called the delayed-self-homodyne technique which typically splits the laser beam into two by either a beam splitter or a fiber coupler and then combines them at a square law detector with a relative time delay τ_d . The total field at the detector is

$$E_T(t) = \frac{E_0}{\sqrt{2}} e^{i[\omega t + \phi(t)]} \{1 + e^{-i\omega\tau_d} e^{i[\phi(t-\tau_d) - \phi(t)]}\} \quad (6.1)$$

The photocurrent at the square law detector is proportional to the square of the electric field and is evaluated as

$$I(t) = s_d I_0 \{1 + \Re\{e^{-i\omega\tau_d} e^{i[\phi(t-\tau_d) - \phi(t)]}\}\} \quad (6.2)$$

The spectral density function of the photocurrent is given by

$$W_I(\Omega) = s_d^2 I_0^2 \left\{ (2 + e^{-2\tau_d/\tau_c}) \delta(\Omega) + \frac{\tau_c [1 - e^{-2\tau_d/\tau_c} (\cos \Omega\tau_d + \frac{2}{\Omega\tau_c} \sin \Omega\tau_d)]}{2\pi (1 + \frac{1}{4}\Omega^2\tau_c^2)} \right\} \quad (6.3)$$

where a detailed derivation for the spectral density function is given in Appendix B. This result holds for arbitrary τ_d and was derived using Wick's theorem. Some interesting observations of this general result are also presented in Appendix B.

When $\tau_d/\tau_c \gg 1$, Equation 6.3 reduces to the well-known result

$$W_I(\Omega) = s_d^2 I_0^2 \left[2\delta(\Omega) + \frac{\tau_c}{2\pi (1 + \frac{1}{4}\Omega^2\tau_c^2)} \right] \quad (6.4)$$

which has a linewidth equivalent to twice that of the laser field [5]. Delayed-self-heterodyne detection in which one beam is delayed and shifted in frequency leads to essentially the same result except that the Lorentzian lineshape is centered at the RF frequency instead of zero frequency.

The experimental setup is shown in Figure 6.1. An Ortel 1610A $1.3\mu m$ distributed feedback laser module (fiber-coupled) was used as the laser source. The measured value of the laser linewidth, for an estimated laser output power of 5mW, is

$$(\Delta\nu)_{laser} \simeq 20 MHz$$

and therefore, the coherence time of the laser is

$$\tau_c = \frac{1}{\pi \Delta\nu_{laser}} \simeq \frac{1.0 \times 10^{-7}}{2\pi} \text{seconds}$$

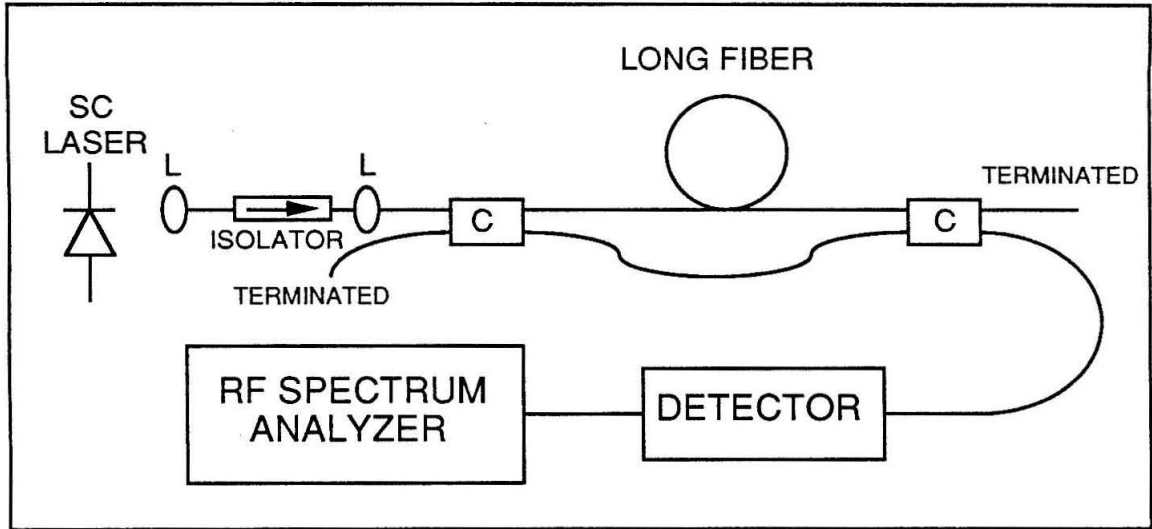


Figure 6.1: The experimental setup for measuring coherence time of a semiconductor laser, where L is micro-objective lens, and C is fiber coupler. The laser output is split into two beams then combines at a square law detector with relative time delay that is much longer than the coherence time. The photocurrent spectrum is analyzed by an RF spectrum analyzer.

With the laser operated at a constant output power (5mW), the intensity noise for the three cases with varying fiber lengths were measured. Constant output power was used resulting from the fact that laser coherence time is proportional to the output power [6].

6.3 Rayleigh Scattering

The experimental study was carried out using an Ortel 1610A $1.3\mu\text{m}$ DFB laser, single-mode fibers of lengths 6.5km and 20km, an Ortel photoreceiver (fiber-coupled) as detector, an HP8590A RF spectrum analyzer, and low reflection optical connectors.

The single-mode fibers used have a loss coefficient

$$\alpha = 0.4dB/km$$

In the experimental setups used in this study, other sources of noise at detection were thoroughly analyzed and the result indicated that the leading non-Rayleigh intensity fluctuations was the shot noise at the detector with the remaining sources of noise being negligible. Therefore, the measured noise level was primarily composed of shot noise and noise due to Rayleigh scattering.

If the photocurrent at the detector (photoreceiver) is I_0 , then the shot noise at the detector [5] is given by

$$\langle I_N^2 \rangle = 2eI_0\Delta\nu \quad (6.5)$$

where $\Delta\nu$ is the bandwidth of the photoreceiver. The relative intensity noise associated with this shot noise is

$$RIN_{shot} = 10 \log \frac{\langle I_N^2 \rangle}{I_0^2 \Delta\nu} = -155.0 - 10 \log I_0 \text{ dB/Hz} \quad (6.6)$$

where I_0 is in mA. In this experimental study the photocurrent I_0 was measured to determine shot noise and the measured RIN is then corrected to represent RIN due to Rayleigh scattering.

To measure the RIN one must determine the noise level and the DC signal level and then take the ratio. Because the photoreceiver used for measurement had a bandwidth from 20MHz to 550MHz, the DC signal power could not be measured directly. Therefore, the laser was modulated by direct current modulation and the

signal level (S_{RF}) at the modulation frequency was measured. The RIN at Ω is given by

$$RIN = \frac{N_{RF}(\Omega)}{2S_{RF}(\Omega)/m^2} \quad (6.7)$$

where N_{RF} and S_{RF} are the noise and signal RF power and m is the amplitude modulation index of the signal S_{RF} which was adjusted to

$$m^2 = 10^{-3}$$

for this study. Therefore, the RIN is given by

$$RIN = -33.0 - 10 \log \frac{S_{RF}}{N_{RF}} \text{ dB/Hz} \quad (6.8)$$

Double Rayleigh scattering in optical fibers

The experimental setup for the case of double Rayleigh scattering in optical fibers is shown in Figure 6.2. The laser light is transmitted through the fibers (with lengths of 6.5km and 20km) and then detected by an Ortel photoreceiver (with built-in amplification circuitry and fiber-coupled) whose signal was then analyzed by an HP8590A RF spectrum analyzer. Figure 6.2 also shows the photocurrent spectrum (with a 20km fiber) where the signal at a frequency of approximately 100MHz was due to a local RF signal detected by the setup which did not cause any difficulty and, therefore, was not an issue of concern.

For $L = 20\text{km}$, the experimental data are shown as follows

$$RIN_{shot} = -154.3\text{dB/Hz}$$

$$S_{RF} = -14.5dB$$

$$N_{RF} = -125.5dB/Hz \quad \text{at } 62.5MHz$$

$$\frac{N_{RF}}{S_{RF}} = -111.0dB/Hz$$

$$RIN = -144.0dB/Hz \quad \text{at } 62.5MHz$$

After correcting for the contribution due to shot noise at the detector, the RIN due to Rayleigh scattering is

$$RIN = -144.5dB/Hz \quad \text{at } 62.5MHz.$$

This data was used to determine the physical parameter S_R using Equation 5.21

$$RIN = 4(\alpha L_{eff}) \left(\frac{\beta^2 k^2 z_R}{n_0^2 \alpha} \right)^2 \frac{\tau_c}{1 + (\frac{1}{2} \Omega \tau_c)^2}$$

yielding a result of

$$S_R = 6.0 \times 10^{-4} \quad (6.9)$$

Using this result, the RIN for other cases was predicted. For a fiber length of $6.5km$, the predicted RIN is $-151.7dB/Hz$ at $62.5MHz$ which is in good agreement with the measured value of $-151.9dB/Hz$ (after correction) where

$$RIN_{shot} = -160.0dB/Hz$$

$$S_{RF} = -3.4dB$$

$$N_{RF} = -121.9dB/Hz \quad \text{at } 62.5MHz$$

$$\frac{N_{RF}}{S_{RF}} = -118.5dB/Hz$$

$$RIN = -151.5dB/Hz \quad \text{at } 62.5MHz$$

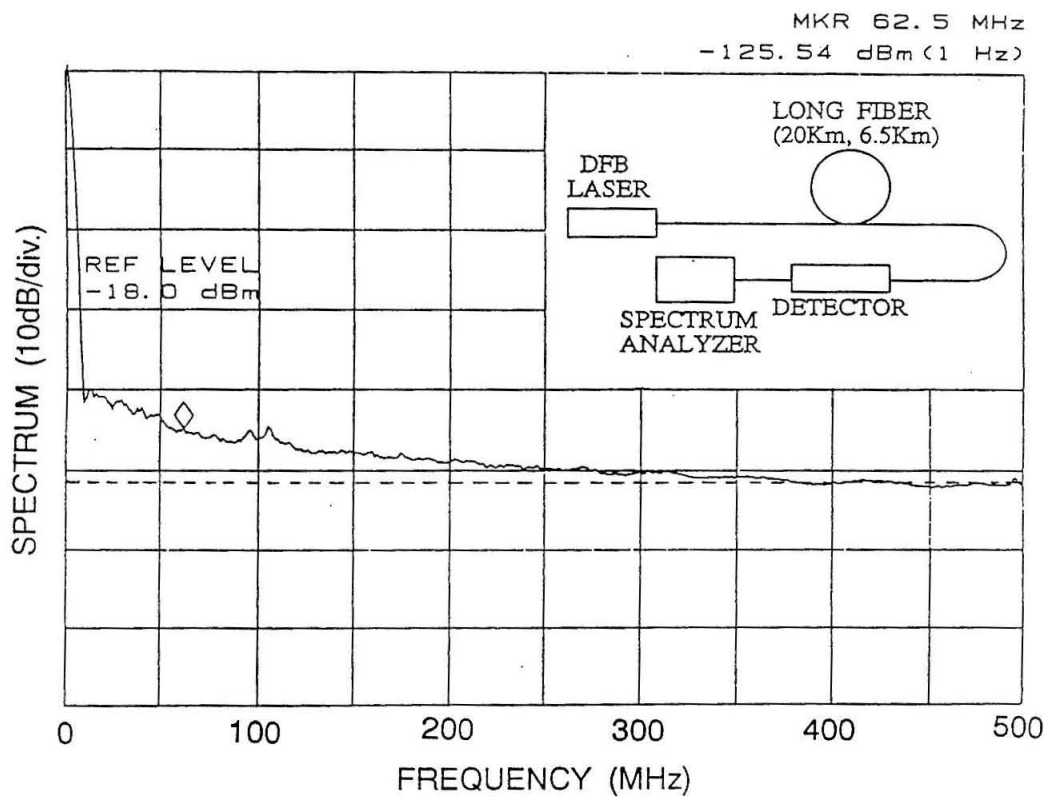


Figure 6.2: Experimental setup and photocurrent spectrum for double Rayleigh scattering in optical fibers.

Redirected Rayleigh scattering in optical fibers

Figure 6.3 shows the photocurrent spectrum ($L = 20km$) and the experimental setup for the case of redirected Rayleigh scattering in optical fibers. A single-mode fiber coupler of 33%/55% transmission was used for the purpose of providing the reflection at the input end of the fiber. There exists approximately a 3.5 % reflection at port 3 due to the fiber-air interface, and port 4 was made to have no reflection.

For a fiber length of 20km, the RF signal level ($\sim -23.4dB$) is shown in Figure 6.4 where the central spike is the sinusoidal signal at 295.2MHz. What is interesting is that the noise spectrum surrounding the signal has a typical Lorentzian lineshape (verified by the measurement) which is identical (as predicted by the theory) to that of the delayed-self-homodyne measurement [7,8]. Therefore, the very phenomenon of Rayleigh scattering in optical fibers can be used as a simple mechanism to measure the laser linewidth and the coherence time. In this case, the laser linewidth was measured and determined to be approximately 20MHz, a value which agrees with the result from the delayed-self-homodyne technique. The shot noise at the detector and the measured RIN are given by the following

$$RIN_{shot} = -149.0dB/Hz$$

$$RIN = -138.2dB/Hz \quad \text{at } 62.5MHz$$

which agrees with the predicted value of $-138.0 \sim -138.7dB/Hz$ where the loss at the optical connectors had been taken into account.

For a fiber length of 6.5km, the results were

$$RIN_{shot} = -155.2dB/Hz$$

$$RIN = -137.3dB/Hz \quad \text{at } 62.5MHz$$

which agrees with the predicted value of $-136.8 \sim -137.5dB/Hz$.

Rayleigh backscattering in optical fibers

Figure 6.5 shows the photocurrent spectrum ($L = 20km$) and the experimental setup for the case of simple Rayleigh backscattering in optical fibers. A single-mode fiber coupler of 33%/55% transmission was used so that the Rayleigh backscattered beam could be detected. Both port 4 of the fiber coupler and the output end of the long fiber were made to have no reflection. The measured RIN was $-87.8dB/Hz$ at $62.5MHz$ which agrees with a predicted value of $87.9dB/Hz$. Notice that the total noise power is the same as the DC power resulting from the fact that the detected signal contains only the Rayleigh scattered signal in this case. The fraction of the incident power reflected due to Rayleigh backscattering was also measured as 0.005 % which agrees with the predicted $0.0044\% \sim 0.0058\%$ where, again, the predicted value is a range instead of a number due to the estimated loss of $0.25 \sim 0.5dB$ at each optical connector.

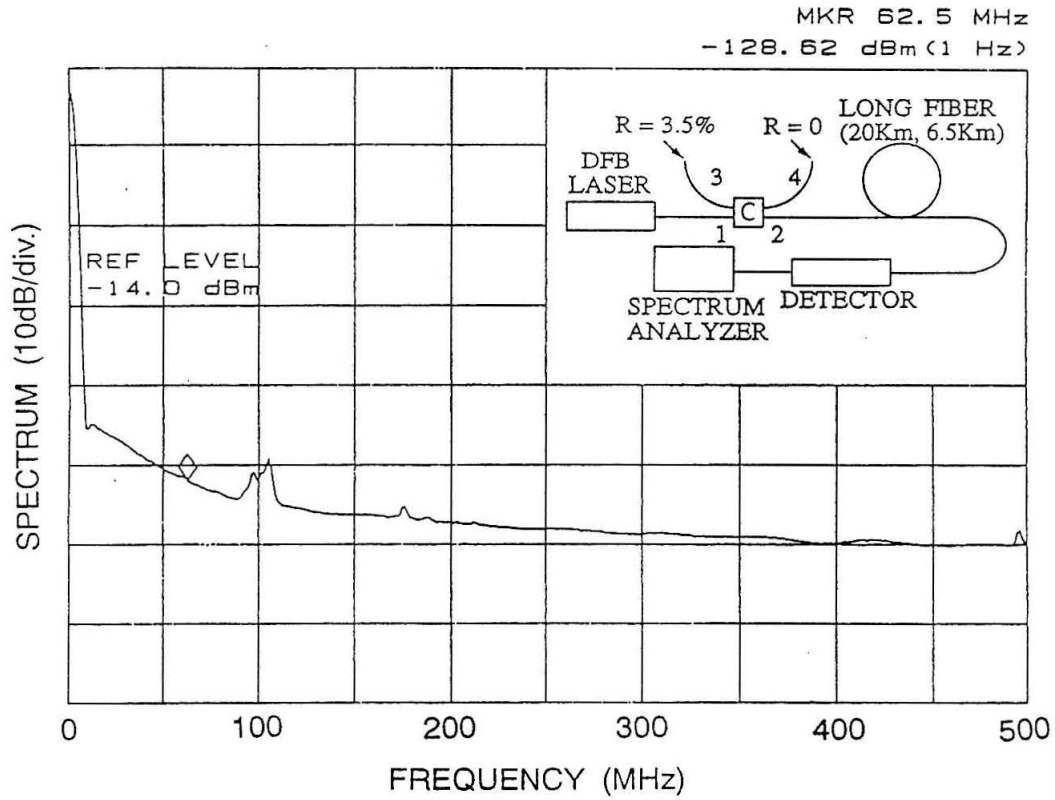


Figure 6.3: Experimental setup and photocurrent spectrum for redirected Rayleigh scattering in optical fibers.

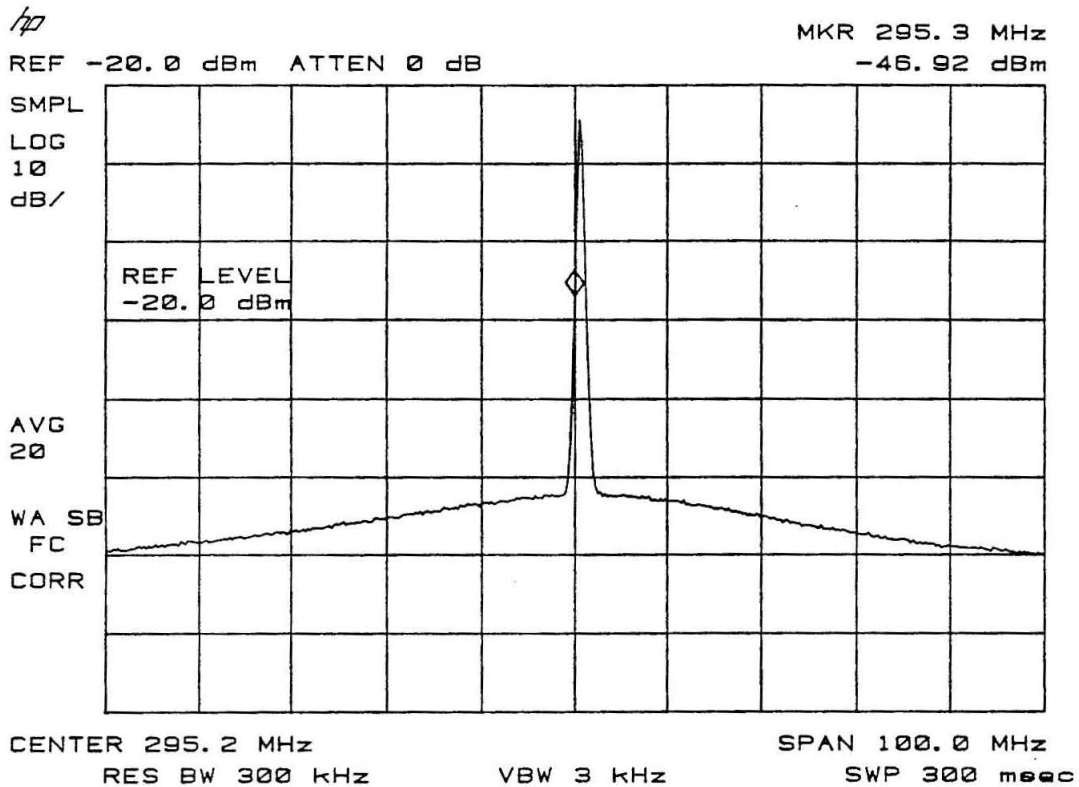


Figure 6.4: Spectrum of the RF signal level and noise surrounding the signal. This demonstrates that Rayleigh scattering in optical fibers can be used to experimentally determine laser linewidth.

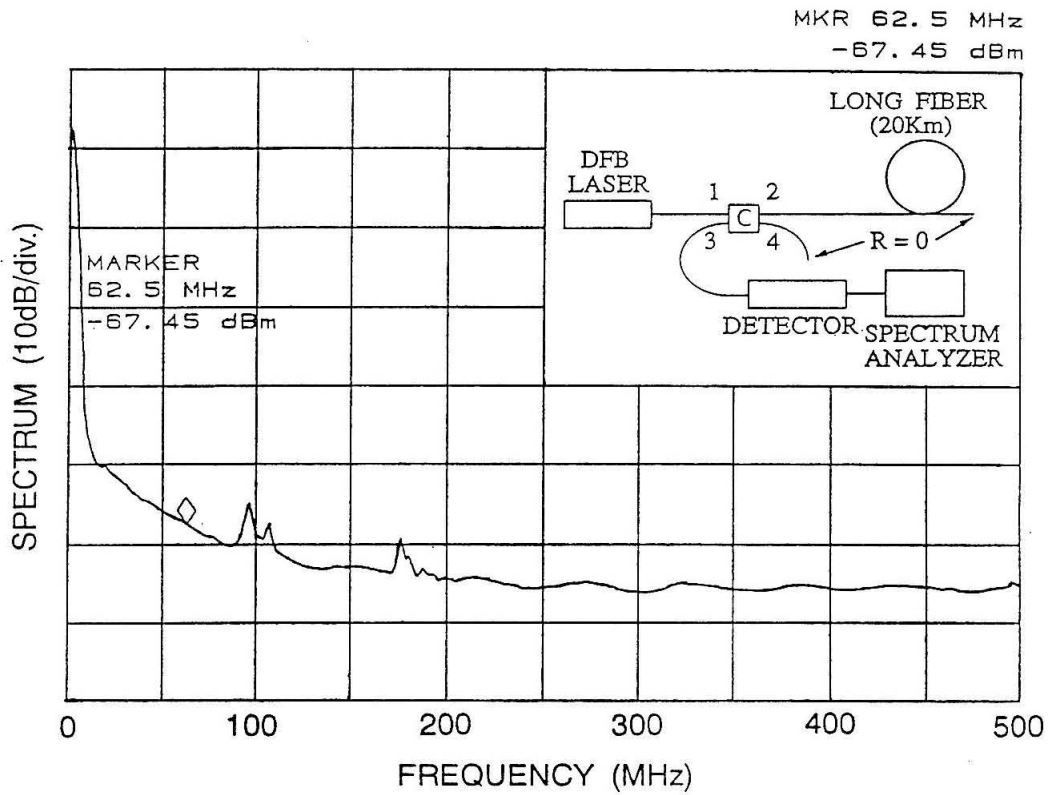


Figure 6.5: Experimental setup and photocurrent spectrum for Rayleigh backscattering in optical fibers.

6.4 Summary

A detailed experimental study of Rayleigh scattering induced phase-to-intensity noise for three different generic cases with varying fiber lengths was conducted. The coherence time was measured using the delayed-self-homodyne measurement technique and the only material parameter, S_R , in the statistical theory was determined using one of the experimental RIN data. The comparison between theoretically predicted and experimentally measured values showed very good agreement within experimental error. It was also experimentally demonstrated that Rayleigh scattering in fibers can be used as an alternative method to measure laser linewidth.

6.5 References

- [1] S. Wu, A. Yariv, H. Blauvelt, and N. Kwong, *Appl. Phys. Lett.*, **59**, 1156(1991).
- [2] A. Yariv, *Optical Electronics*, 4th ed. (Holt, Rinehart and Winston, Philadelphia, 1991).
- [3] Y. Yamamoto, T. Mukai, and S. Saito, *Electron. Lett.*, **17**, 327(1981).
- [4] T. Okoshi, K. Kikuchi, and A. Nakayma, *Electron. Lett.*, **6**, 630(1980).
- [5] A. Yariv, *Quantum Electronics*, 3rd ed. (John Wiley & Sons, New York, 1989).
- [6] L. Schawlow and C. H. Townes, *Phys. Rev.*, **112**, 1940(1958).
- [7] P. Gysel and R. K. Staubli, *IEEE Photon. Tech. Lett.*, **1**, 327(1989).
- [8] S. Wu, A. Yariv, H. Blauvelt, and N. Kwong, "A theoretical study of phase-to-intensity conversion noise by Rayleigh scattering in optical fiber links," to be published.

Chapter 7

Rayleigh Scattering in Fiber Links with Periodic Optical Amplification and a Proposed Noise Reduction Scheme

7.1 Fiber Links with Periodic Optical Amplification

In recent years we have witnessed a major expansion in the field of commercial long haul fiber-optic telecommunications, where signals are transmitted through optical fibers of lengths up to many thousand kilometers. In such systems, periodic ampli-

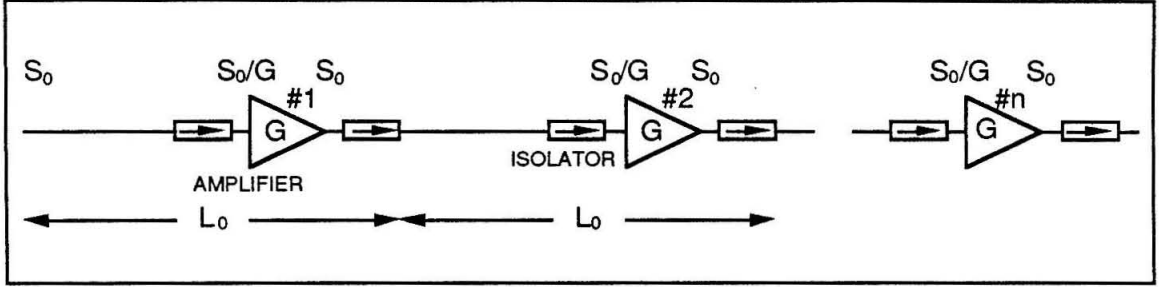


Figure 7.1: Fiber links with n -stage periodic optical amplification. S_0 is the input signal power, L_0 is fiber length between neighboring amplifiers, G is the amplifier gain, and the optical isolators are right before and after each amplifier.

fication of the signals is required to prevent the signal-to-noise ratio from decaying exponentially [1,3,4,6].

Consider a fiber link with n -stage periodic optical amplification (see Figure 7.1), where the incident signal power is S_0 . The signal is attenuated, due to optical loss, by a factor of

$$G^{-1} \equiv e^{-\alpha L_0}$$

in the distance L_0 between amplifiers and is boosted, by the gain $G = e^{\alpha L_0}$ at each amplifier, back up to the original level S_0 . The detected signal power at the output is

$$\langle I_s^2 \rangle_{out} = \left(\frac{S_0 e}{h\nu} \right)^2 \quad (7.1)$$

where e is the electronic charge, $h\nu$ is the photon energy, and a unity detector quantum efficiency is assumed.

Besides the Rayleigh scattering induced noise, to be determined later in this section, the leading output noise current includes:

1. The shot noise [5]

$$\langle I_{shot}^2 \rangle_{out} = \frac{2e^2 S_0}{h\nu} \Delta\nu \quad (7.2)$$

where $\Delta\nu$ is the amplifier bandwidth.

2. The beating between the signal optical field and that of the amplifier spontaneous emission [6]

$$\langle I_n^2 \rangle_{sig-ASE} = \frac{4e^2(G-1)S_0\mu\Delta\nu}{h\nu} \quad (7.3)$$

where

$$\mu = \frac{N_2}{N_2 - N_1 \frac{g_2}{g_1}}$$

is the inversion factor of the optical amplifier.

Consider the phase-to-intensity conversion noise due to Rayleigh scattering [7].

The resulting noise current due to one stage, using Equation 5.20, is given by

$$\langle I_{RS}^2 \rangle_1 = 4S_R^2(\alpha L_{eff}) \frac{e^2 e^{-2\alpha L_0} S_0^2}{(h\nu)^2} G^2 = 4S_R^2(\alpha L_{eff}) \frac{e^2 S_0^2}{(h\nu)^2} \quad (7.4)$$

where

$$L_{eff} = L_0 - \frac{1}{2\alpha}(1 - e^{-2\alpha L_0}) \quad (7.5)$$

The total contribution from n-stages is simply the sum of that from each stage due to the presence of optical isolators before and after each amplifier. Consequently, the total noise current at the detection due to Rayleigh scattering is

$$\langle I_{RS}^2 \rangle = 4S_R^2(n\alpha L_{eff}) \frac{e^2 S_0^2}{(h\nu)^2} \quad (7.6)$$

where $n = L/L_0$, and L is the total length of the fiber link.

The output signal-to-noise ratio is then

$$SNR = \frac{S_0}{2h\nu\Delta\nu[1 + 2n\mu(e^{\alpha L_0} - 1)] + 4S_R^2 n(\alpha L_{eff})S_0} \quad (7.7)$$

which has a n^{-1} dependence due to both the sig-ASE and Rayleigh scattering terms when $G = e^{\alpha L_0} \gg 1$.

It is interesting to compare the sig-ASE and Rayleigh scattering noise currents. From Equations 7.3, and 7.6 it can be seen that both have a linear n dependence and increase as L_0 increases. However, the former depends linearly on the signal power S_0 while the latter is proportional to square of the signal power. Taking the ratio

$$\frac{\langle I_{RS}^2 \rangle}{\langle I_{sig-ASE}^2 \rangle} = \frac{[\alpha L_0 - \frac{1}{2}(1 - e^{-2\alpha L_0})]S_R^2 S_0}{(e^{\alpha L_0} - 1)\mu h\nu\Delta\nu} \quad (7.8)$$

and considering

1. $\alpha L_0 \ll 1$

$$\frac{\langle I_{RS}^2 \rangle}{\langle I_{sig-ASE}^2 \rangle} = \alpha L_0 \frac{S_R^2 S_0}{\mu h\nu\Delta\nu} \xrightarrow{\alpha L_0 \rightarrow 0} 0 \quad (7.9)$$

2. $\alpha L_0 \gg 1$

$$\frac{\langle I_{RS}^2 \rangle}{\langle I_{sig-ASE}^2 \rangle} = \frac{\alpha L_0}{e^{\alpha L_0}} \frac{S_R^2 S_0}{\mu h\nu\Delta\nu} \xrightarrow{\alpha L_0 \rightarrow \infty} 0 \quad (7.10)$$

Consequently, a maximum value of the ratio exists. A realistic numerical estimate is given as follows

$$\lambda = 1.55\mu m$$

$$L_0 = \frac{2}{\alpha} = 43.52 km$$

$$\mu = 1$$

$$\Delta\nu = 10^9 \text{ Hz}$$

$$S_R \propto \frac{1}{\lambda^2 \alpha} \simeq 6.0 \times 10^{-4}$$

$$S_0 = 5 \text{ mW} \times 10\% \text{ modulation}$$

$$\frac{\langle I_{RS}^2 \rangle}{\langle I_{sig-ASE}^2 \rangle} = 0.6$$

It can be seen that Rayleigh scattering contributes a significant and comparable amount of noise as signal-ASE noise in the fiber link under consideration.

It is interesting to calculate the noise current due to Rayleigh scattering when all optical isolators in the fiber link are removed. First, the other noise current terms are not affected. But Rayleigh scattering induced noise is now given by

$$\langle I_{RS}^2 \rangle = 4S_R^2(\alpha L_{eff}) \frac{e^2 S_0^2}{(h\nu)^2} [n + n(n-1)] = 4n^2 S_R^2(\alpha L_{eff}) \frac{e^2 S_0^2}{(h\nu)^2} \quad (7.11)$$

which is n times as large as that for the same fiber link with optical isolators.

The n^2 dependence of the Rayleigh scattering contribution will dominate in fiber links with many stages ($n \gg 1$) and the signal-to-noise ratio will decay as n^{-2} . This is an important observation in light of the fact that substantial effort is being put forth to design semiconductor lasers with high endurance level against optical feedback such that optical isolators in very long haul fiber-optic telecommunication systems can be eliminated. Obviously, the elimination of optical isolators from such systems will substantially reduce the practical implementation cost which now stands as one of the main obstacles for large scale commercial exploitation of fiber-optic communication technologies. The noise current due to beating between signal and the amplifier spontaneous emission is intrinsic to the system and is hard, if not impossible, to

be reduced. However, fortunately the noise term due to Rayleigh scattering can be reduced substantially by pre-phase modulation of the optical field at high frequencies. This will be addressed in the next section.

7.2 Reduction of Rayleigh Scattering Induced Noise by Pre-Phase Modulation of the Optical Field

In this section a noise reduction scheme for long haul fiber-optic amplitude modulation (AM) systems is presented [8]. Such systems suffer from intensity noise which results from interference between the (twice) Rayleigh scattered light and the directly transmitted beam. When the fiber length exceeds the laser coherence distance this interference converts the fundamental phase noise of the laser to intensity noise. It will be demonstrated that a strong phase modulation of the laser output causes a large reduction of the detected signal noise at frequencies near those of the signal components.

As has been previously shown, the interference between light which has been retroreflected twice by Rayleigh scattering and the main beam converts the output phase fluctuations of the laser field to intensity fluctuations at the output of a long ($L > \alpha^{-1}$, where α is the loss coefficient) fiber. The spectrum of this noise consists of a base band extending from zero to roughly twice the laser linewidth ($\Delta\nu_{laser}$). If the laser is modulated by information at frequencies exceeding $\Delta\nu_{laser}$, then the spectrum of the detected intensity will consist of similar noise pedestals straddling

each modulation frequency resulting from beating between information sidebands and the carrier. This, in turn, degrades the signal-to-noise ratio of the detected AM signal.

From the fact that modulation will generate noise sidebands about the modulation frequency and higher harmonics, intuitively, one should expect to achieve *local* noise reduction when modulation is introduced. The analysis which follows shows how the detected signal-to-noise ratio at the output of long fibers can be improved by strong phase modulation of the signal prior to launching into the fiber.

Consider a laser diode (LD) operating continuously (CW) without internal modulation. The message (signal) one desires to transmit is encoded by external amplitude modulation (AM) at ω_m (typically a few hundred MHz). Normally the laser beam is coupled into a long single-mode fiber in an optical telecommunication system. As a mechanism to reduce intensity fluctuations at the output end of the fiber due to mixing between direct transmitted light and Rayleigh scattered light, an external phase modulation [9] is introduced at Ω_m ($\gg \omega_m$), as shown in Figure 7.2.

The analytic signal of the laser field, before coupling to the fiber, is given by

$$E(0, t) = E_0(1 + m \cos \omega_m t) e^{i[\omega t + \delta \cos \Omega_m t + \phi(t)]} \quad (7.12)$$

where m is the (information) AM modulation index, ω_m is the AM (signal) modulation frequency, δ is the phase modulation index, and Ω_m is the phase modulation frequency. The phase fluctuation is characterized by (see Equation 5.2)

$$\langle \Delta\phi(\tau_1) \Delta\phi(\tau_2) \rangle = \frac{2}{\tau_c} \min(\tau_1, \tau_2) \quad (7.13)$$

The total field at the detector is the sum of the “direct” beam and the doubly

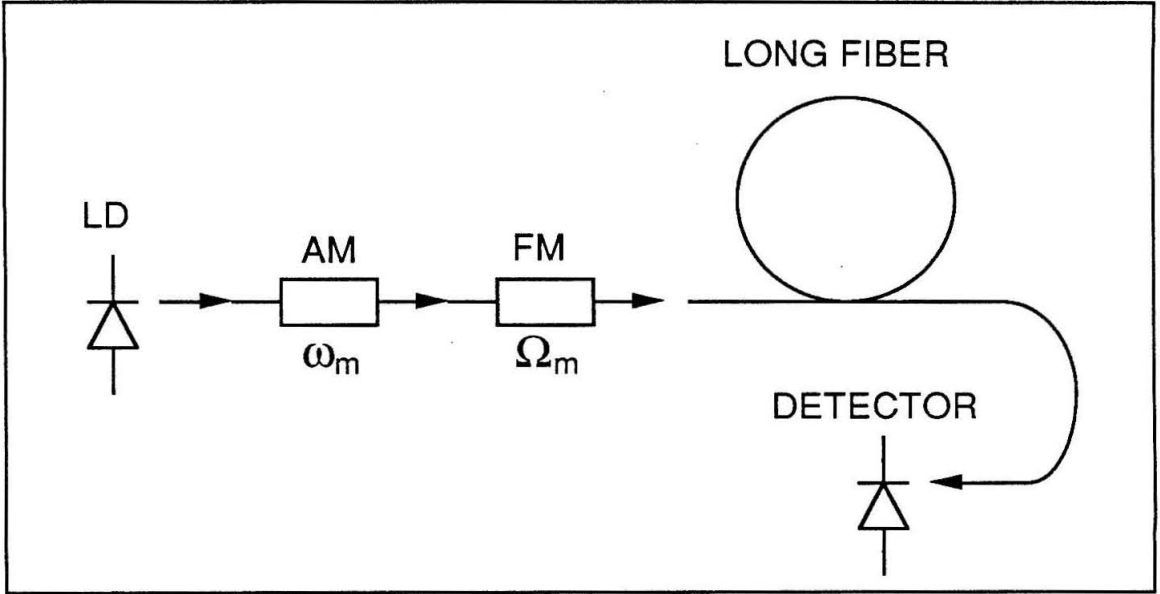


Figure 7.2: The optical system under study: LD operating at CW, signal encoded by AM modulation at ω_m , an FM modulation at frequency Ω_m , and laser light transmitted through a long single-mode fiber and finally detected.

scattered beam

$$E_T(L, t) = E_0(L, t) + E_{ds}(L, t) \quad (7.14)$$

where

$$E_0(L, t) = E_0(1 + m \cos \omega_m t) e^{-\alpha L/2} e^{i[\omega t + \delta \cos \Omega_m t + \phi(t)]} \quad (7.15)$$

$$\begin{aligned} E_{ds}(L, t) = & E_0 e^{i\omega t} e^{-\alpha L/2} \left(-\frac{1}{4n_0^2} \right) \sum_{j=1}^{L/a} \sum_{j'=0}^{j-1} (\Delta n_{j+1} - \Delta n_j) (\Delta n_{j'+1} - \Delta n_{j'}) \\ & \cdot \left\{ 1 + m \cos \omega_m \left[t - \frac{2(j-j')a}{v} \right] \right\} e^{-(\alpha+2ik)(j-j')a} \\ & \cdot e^{i\phi \left[t - \frac{2(j-j')a}{v} \right]} e^{i\delta \cos \Omega_m \left[t - \frac{2(j-j')a}{v} \right]} \end{aligned} \quad (7.16)$$

The photocurrent at the detector is proportional to the product of $E_T(L, t)$ and its complex conjugate

$$I(t) = s_d I_0 e^{-\alpha L} [(1 + m \cos \omega_m t)^2 + g(t) + g^*(t)] \quad (7.17)$$

where

$$\begin{aligned}
g(t) = & -\frac{1}{4n_0^2} \sum_{j=1}^{L/a} \sum_{j'=0}^{j-1} (\Delta n_{j+1} - \Delta n_j)(\Delta n_{j'+1} - \Delta n_{j'}) e^{-(\alpha+2ik)(j-j')a} \\
& \cdot (1 + m \cos \omega_m t) \left\{ 1 + m \cos \omega_m \left[t - \frac{2(j-j')a}{v} \right] \right\} \\
& \cdot e^{i\{\phi[t-\frac{2(j-j')a}{v}] - \phi(t)\}} e^{i\delta\{\cos \Omega_m[t-\frac{2(j-j')a}{v}] - \cos \Omega_m t\}}
\end{aligned} \tag{7.18}$$

The photocurrent autocorrelation function, defined as

$$C(\tau) = \langle I(t)I(t+\tau) \rangle$$

is evaluated using Equations 7.17 and 7.18. By neglecting the small correction terms (second and fourth order in $\Delta n(z)$) to the DC, signal at ω_m , and signal at $2\omega_m$, we have

$$\begin{aligned}
C(\tau) = & s_d^2 I_0^2 e^{-2\alpha L} \left\{ \left(1 + \frac{m^2}{2}\right)^2 + 2m^2 \cos \omega_m \tau + \frac{m^4}{8} \cos 2\omega_m \tau \right. \\
& \left. + 2\Re \langle g(t)g^*(t+\tau) \rangle \right\}
\end{aligned} \tag{7.19}$$

In evaluating $\langle g(t)g^*(t+\tau) \rangle$, one encounters:

1. Fourth order correlation functions which are evaluated using Wick's theorem (see Appendix A).
2. The factors due to AM and phase modulation

$$\begin{aligned}
& \langle [1 + m \cos \omega_m(t+\tau)][1 + m \cos \omega_m(t - \frac{2x}{v})][1 + m \cos \omega_m(t+\tau - \frac{2x}{v})] \\
& \cdot (1 + m \cos \omega_m t) e^{i\delta\{\cos \Omega_m(t-\frac{2x}{v}) - \cos \Omega_m t - \cos \Omega_m(t+\tau-\frac{2x}{v}) + \cos \Omega_m(t+\tau)\}} \rangle \\
& = [1 + \frac{m^4}{8} + m^2 \cos \omega_m \tau + \frac{m^4}{8} \cos 2\omega_m \tau] J_0[4\delta \sin(\frac{\Omega_m \tau}{2}) \sin(k_m x)]
\end{aligned} \tag{7.20}$$

where, $k_m \equiv \Omega_m/v$, J_0 is the zeroth order Bessel function.

3. The quadruple integrations over the fiber length that is approximated using the inequalities $v\tau_c \gg 1/k \gg z_R$ ($v\tau_c \sim 1$ meter, $1/k \sim 2000 \text{ \AA}$, $z_R \sim 100 \text{ \AA}$ in practical systems).

Lengthy, but straightforward, algebra yields

$$C(\tau) = s_d^2 I_0^2 e^{-2\alpha L} \left\{ \left(1 + \frac{m^2}{2}\right)^2 + 2m^2 \cos \omega_m \tau + \frac{m^4}{8} \cos 2\omega_m \tau + 4S_R^2 (\alpha L_{eff}) e^{-2\tau/\tau_c} \right. \\ \left. \cdot \left[1 + \frac{m^4}{8} + m^2 \cos \omega_m \tau + \frac{m^4}{8} \cos 2\omega_m \tau\right] [f(\delta) + \dots] \right\} \quad (7.21)$$

where

$$S_R = \frac{\beta^2 k^2 z_R}{n_0^2 \alpha} \quad (7.22)$$

$$L_{eff} = L - \frac{1}{2\alpha} (1 - e^{-2\alpha L}) \quad (7.23)$$

$$f(\delta) = \sum_{l=0}^{\infty} (-1)^l \left[\frac{(2l)!}{2^l (l!)^3} \right]^2 \delta^{2l} \quad (7.24)$$

and the omitted terms are higher Fourier components of $\Omega_m \tau$.

The spectral density function $W_I(\Omega)$ of the detected photocurrent at frequency Ω is obtained using the Wiener-Khintchine theorem

$$W_I(\Omega) = \frac{2}{\pi} \int_0^{\infty} C(\tau) \cos \Omega \tau d\tau \quad (7.25)$$

and is evaluated using Equation 7.21, yielding

$$W_I(\Omega) = s_d^2 I_0^2 e^{-2\alpha L} \left\{ \left(1 + \frac{m^2}{2}\right)^2 \delta(\Omega) + 2m^2 \delta(\Omega - \omega_m) + \frac{m^4}{8} \delta(\Omega - 2\omega_m) \right. \\ \left. + 4S_R^2 (\alpha L_{eff}) f(\delta) \left[\left(1 + \frac{m^4}{8}\right) \frac{\tau_c/\pi}{1 + \frac{1}{4}\Omega^2 \tau_c^2} + m^2 \frac{\tau_c/2\pi}{1 + \frac{1}{4}(\Omega - \omega_m)^2 \tau_c^2} \right. \right. \\ \left. \left. + \frac{m^4}{8} \frac{\tau_c/2\pi}{1 + \frac{1}{4}(\Omega - 2\omega_m)^2 \tau_c^2} \right] + \dots \right\} \quad (7.26)$$

where

1. The “delta” function $\delta(\Omega)$, $\delta(\Omega - \omega_m)$, and $\delta(\Omega - 2\omega_m)$ terms represent the DC, signal at ω_m , and signal at $2\omega_m$, respectively.

2. The term

$$\frac{\tau_c/2\pi}{1 + \frac{1}{4}(\Omega - \omega_m)^2\tau_c^2}$$

represents the Lorentzian noise spectrum straddling the signal at ω_m .

3. The omitted terms are the noise spectra around frequencies $n\Omega_m + j\omega_m$, $n = 1, 2, 3, \dots$, and $j = \pm 1, \pm 2$.

From Equation 7.26, the noise-to-signal ratio (at $\Omega = \omega_m$) is given by

$$\frac{N}{S} = 2S_R^2(\alpha L_{eff})f(\delta) \int_{\omega_m - \frac{\Delta\Omega}{2}}^{\omega_m + \frac{\Delta\Omega}{2}} U(\Omega)d\Omega \quad (7.27)$$

where $\Delta\Omega$ is the bandwidth of the detection circuit and $U(\Omega)$ is the (unity) normalized Lorentzian lineshape function

$$U(\Omega) = \frac{\tau_c/2\pi}{1 + \frac{1}{4}(\Omega - \omega_m)^2\tau_c^2} = \frac{\frac{2}{\pi\Delta\Omega_{1/2}}}{1 + \frac{4(\Omega - \omega_m)^2}{(\Delta\Omega_{1/2})^2}} \quad (7.28)$$

and $\Delta\Omega_{1/2} = 4/\tau_c$ is twice the FWHM optical linewidth of the laser output.

It is interesting to obtain an estimate of the noise-to-signal ratio in a practical system (e.g., fiber-optic cable TV system) without phase modulation at Ω_m , i.e., $f(\delta) =$

1. Using experimental data from Chapter 6, $\alpha = 0.4dB/km$, $2\pi\tau_c = 1.0 \times 10^{-7}$ seconds, and $S_R = 6.0 \times 10^{-4}$, for $L = 20km$ and $\Delta\Omega = 6MHz$ (per channel), a noise-to-signal ratio of $-72.4dB$ at $\Omega = \omega_m$ is calculated using Equation 7.27. This phase-to-intensity conversion noise, the largest noise source in the systems under study, limits the ultimate noise-to-signal performance.

With phase modulation at Ω_m , the noise level is reduced by the factor $f(\delta)$ given by Equation 7.24. A plot of $f(\delta)$ vs δ is shown in Figure 7.3, where it can be seen that the noise level can be reduced by as much as $10dB$ at $\delta \approx 6$. Physically, this can be interpreted as due to the fact that the external phase modulation at high frequency generates optical sidebands which effectively distribute the laser and the detected intensity noise over a large frequency interval. Consequently, the local noise level near the signal frequency (ω_m) is reduced.

Although our analysis is specific to the case of a fiber, it is clear that any optical system in which interference of a laser field with a delayed part of itself converts phase noise to amplitude noise will benefit from a pre-phase modulation of the optical carrier [10]. In this section, the analysis has been conducted under the condition of $\Omega_m \gg \omega_m$, but it should be understood that, mathematically, the same reduction in noise can be achieved under the less restrictive condition that

$$|n\Omega_m + j\omega_m| \gg \Omega_{1/2} = \frac{4}{\tau_c} \quad (7.29)$$

$$n = 1, 2, 3, \dots$$

$$j = \pm 1, \pm 2, \pm 3.$$

For an actual system that transmits many AM signals at different frequencies (e.g., a typical fiber-optic cable TV system carrying many channels, bandwidth 100MHz-550MHz, 6MHz per channel), the only way for Equation 7.29 to be satisfied for all ω_m s is when $\Omega_m \gg \omega_m$ (practically, $\Omega_m > 3\omega_m$ is acceptable). It may be instructive to compare the phase modulation scheme to those employing “low-coherence lasers.”

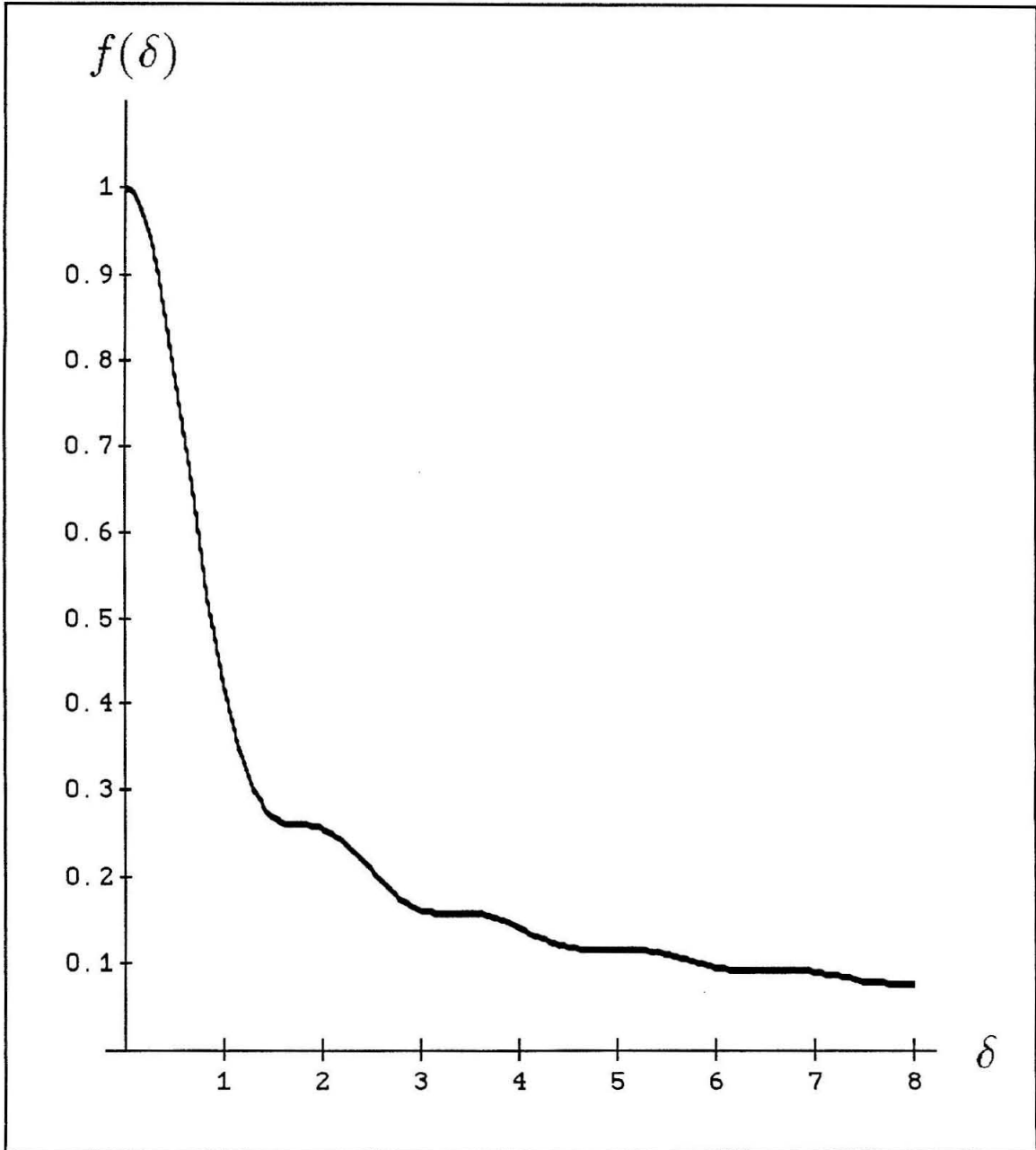


Figure 7.3: A plot of $f(\delta)$ versus δ (using *Mathematica*). The first 50 terms of Equation 7.24 are included. $f(\delta) = 0.1$ when $\delta \approx 6$.

The latter usually achieve their state of low coherence by random phase modulation. If the spectrum of this modulation is comparable or smaller than the information bandwidth there is no improvement in the detected intensity noise. To obtain a reduction of the noise it is necessary that the coherence time be much shorter than the inverse of the information bandwidth. However, this is essentially what is achieved by the phase modulation scheme where $\delta\Omega_m \gg \omega_m$. The effect of fiber chromatic dispersion on the heavily phase-chirped signal can be avoided by choosing the laser wavelength ($1.3\mu m$) at which the fiber has zero dispersion [11].

In conclusion, the intensity fluctuation spectral density due to Rayleigh scattering in long haul fiber-optic telecommunication systems can be substantially reduced by external phase modulation at very high frequencies.

7.3 Comments on Future Work Related to Rayleigh Scattering in Optical Fibers

Lately, there has been substantial activity in using optical feedback from single-mode fiber ring due to Rayleigh backscattering to achieve laser linewidth reduction. This certainly offers an interesting prospect that by simply inserting a single-mode fiber ring in fiber links, without any extra effort, semiconductor laser linewidth will be reduced. Thus far, the experimental work by Paul and Swanson demonstrated that the reduction in laser linewidth is stable only after careful reduction of ambient acoustic and thermal disturbances are implemented [12]. Obviously, further research along

that direction needs to be conducted.

There has also been some effort in designing a DFB laser which will be more tolerable to optical feedback [13]. The purpose is to eliminate the optical isolators in fiber links. Since the optical feedback due to discrete reflections in fiber links can in principle be eliminated, Rayleigh backscattering would result in the only unavoidable optical feedback. In designing lasers with higher endurance against optical feedback, the effect of Rayleigh backscattering has to be considered. Furthermore, the quadratic accumulation [7] of the intensity noise due to Rayleigh scattering in a long haul fiber links without optical isolator must be addressed. Some noise reduction scheme must be implemented.

7.4 References

- [1] J. C. Simon, *J. Opt. Commun.*, **4**, 51(1983).
- [2] R. J. Mears, L. Reekie, I. M. Jauncey, and D. N. Payne, *Electron. Lett.*, **23**, 1026(1987).
- [3] K. Hagimoto, et al., *Proceedings of the Optical Fiber Conference*, Houston, TX, postdeadline paper PD15, 1989.
- [4] A. Yariv, *Opt. Lett.*, **15**, 1064(1990).
- [5] A. Yariv, *Optical Electronics*, 4th ed. (Holt, Rinehart and Winston, Philadelphia, 1991).
- [6] R. J. Mears, L. Reekie, I. M. Jauncey, and D. N. Payne, *Electron. Lett.*, **23**, 1026(1987).
- [7] S. Wu, A. Yariv, H. Blauvelt, and N. Kwong, "A theoretical study of phase-to-intensity conversion noise by Rayleigh scattering in optical fiber links," to be published.
- [8] A. Yariv, H. Blauvelt, and S. Wu, "Reduction of interferometric phase-to-intensity conversion noise in fiber links by large index phase modulation of the optical beam," accepted to be published in *J. Lightwave. Tech.*, **10**, July, 1992.
- [9] A. Yariv, *Quantum Electronics*, 3rd ed. (John Wiley & Sons, New York, 1989).
- [10] P. K. Pepeljugoski and K. Y. Lau., to be published.

- [11] D. L. Frazen, *Proceedings of the Tutorial Sessions on Optical Fiber Communications*, Washington, D.C., Opt. Soc. Am., 101(1988).
- [12] T. J. Paul and E. A. Swanson, presented at *OFC'92*, paper TuM5.
- [13] T. Kurosaki, T. Hirono, and M. Fukuda, presented at *OFC'92*, paper FB4.

Appendix A

Wick's Theorem

Wick's theorem is very commonly used in field theory where it is applied to express a time-ordered operator product in terms of a normal-ordered operator product and Feynman propagator. To translate this into more familiar terms for a non-expert in field theory, a Feynman propagator is equivalent to what is called second order correlation function in statistical physics. A normal-ordered operator has zero expectation value by definition. Therefore, a narrower application of Wick's theorem is to express higher order correlation functions in terms of mean (average) and second order correlation function. Wick's theorem applies to statistical systems in equilibrium with a quadratic time-independent Hamiltonian. This is apparent when the path integral approach to statistical mechanics is used.

Consider a random variable $x(t)$ whose statistical average is zero. Wick's theorem

can be narrowly stated as

$$\langle x(t_1)x(t_2)\cdots x(t_{n-1})x(t_n) \rangle = \langle x(t_1)x(t_2) \rangle \cdots \langle x(t_{n-1})x(t_n) \rangle + \text{permutation} \quad (\text{A.1})$$

where n is an even integer. Specifically, for a fourth order correlation function, we have

$$\begin{aligned} \langle x(t_1)x(t_2)x(t_3)x(t_4) \rangle &= \langle x(t_1)x(t_2) \rangle \langle x(t_3)x(t_4) \rangle \\ &+ \langle x(t_1)x(t_3) \rangle \langle x(t_2)x(t_4) \rangle \\ &+ \langle x(t_1)x(t_4) \rangle \langle x(t_2)x(t_3) \rangle \end{aligned} \quad (\text{A.2})$$

To demonstrate the power of Wick's theorem, an example is given as follows. Consider the random phase fluctuations in semiconductor lasers. The random variable $\Delta\phi$ represents phase fluctuations resulting from many independent spontaneous emission events and, therefore, according to the central limit theorem, obeys Gaussian statistics. Consequently, Wick's theorem is applicable. In calculating the laser field spectrum, the correlation function

$$\langle e^{i\Delta\phi(t,\tau)} \rangle$$

is encountered, where

$$\Delta\phi(t,\tau) \equiv \phi(t+\tau) - \phi(t) \quad (\text{A.3})$$

$$\langle [\Delta\phi(t,\tau)]^2 \rangle = \frac{2}{\tau_c} |\tau| \quad (\text{A.4})$$

Using the Taylor series expansion, we obtain

$$\langle e^{i\Delta\phi(t,\tau)} \rangle = 1 + \sum_{n=1}^{\infty} \frac{\langle [i\Delta\phi(t,\tau)]^n \rangle}{n!}$$

$$= 1 + \sum_{k=1}^{\infty} \frac{\langle [i\Delta\phi(t, \tau)]^{2k} \rangle}{(2k)!} \quad (\text{A.5})$$

The $2k^{\text{th}}$ order correlation function can be evaluated, using Wick's theorem, as

$$\begin{aligned} \langle [\Delta\phi(t, \tau)]^{2k} \rangle &= (2k-1)(2k-3)\cdots 1 \langle [\Delta\phi(t, \tau)]^2 \rangle^k \\ &= (2k-1)!! \langle [\Delta\phi(t, \tau)]^2 \rangle^k \end{aligned} \quad (\text{A.6})$$

Therefore,

$$\begin{aligned} \langle e^{i\Delta\phi(t, \tau)} \rangle &= 1 + \sum_{k=1}^{\infty} \frac{(-1)^k (2k-1)!! \langle [\Delta\phi(t, \tau)]^2 \rangle^k}{(2k)!} \\ &= 1 + \sum_{k=1}^{\infty} \frac{(-1)^k \langle [\Delta\phi(t, \tau)]^2 \rangle^k}{(2k)!!} \\ &= 1 + \sum_{k=1}^{\infty} \frac{(-1)^k \langle [\Delta\phi(t, \tau)]^2 \rangle^k}{2^k k!} \\ &= e^{-\frac{\langle [\Delta\phi(t, \tau)]^2 \rangle}{2}} \\ &= e^{-\frac{|z|}{\tau_c}} \end{aligned} \quad (\text{A.7})$$

This result can be generalized as

$$\langle e^{i\sum_{k=1}^n \Delta\phi(t, \tau_k)} \rangle = e^{-\langle [\sum_{k=1}^n \Delta\phi(t, \tau_k)]^2 \rangle / 2} \quad (\text{A.8})$$

which is a useful result for Section 5.3 where a similar correlation function with $n = 3$ was encountered.

References

- [1] J. D. Bjorken and S. D. Drell, *Relativistic Quantum Fields*, (McGraw-Hill, New York, 1965).
- [2] A. R. Hibbs and R. P. Feynman, *Quantum Mechanics and Path Integrals*, (McGraw-Hill, New York, 1965).

Appendix B

Delayed-Self-Homodyne Measurement Technique

In a delayed-self-homodyne measurement of linewidth (for experimental setup, see Figure 6.1), the laser beam is split into two which is then combined at a square law detector with a relative time delay τ_d . The electric field at the square law detector is given by

$$E(t) = \frac{E_0}{\sqrt{2}} e^{i[\omega t + \phi(t)]} \{1 + e^{-i\omega\tau_d} e^{[\phi(t-\tau_d) - \phi(t)]}\} \quad (\text{B.1})$$

The photocurrent is proportional to the incident optical intensity, and is evaluated as

$$I(t) = s_d I_0 \{1 + \Re\{e^{[\phi(t-\tau_d) - \phi(t)]}\}\} \quad (\text{B.2})$$

Therefore, the autocorrelation function of the photocurrent can be calculated as follows

$$C_I(\tau) = \langle I(t)I(t + \tau) \rangle$$

$$\begin{aligned}
&= s_d^2 I_0^2 \left\{ 1 + \frac{1}{2} \Re \langle e^{i[\phi(t-\tau_d) - \phi(t) - \phi(t+\tau-\tau_d) + \phi(t+\tau)]} \rangle \right\} \\
&= s_d^2 I_0^2 \left[1 + \frac{1}{2} e^{-\frac{2}{\tau_c} \min(\tau, \tau_d)} \right] \tag{B.3}
\end{aligned}$$

where Wick's theorem and Equation 5.3 are used. The spectral density function of the photocurrent is the Fourier transform of $C_I(\Omega)$. After straightforward algebra, we obtain

$$W_I(\Omega) = s_d^2 I_0^2 \left\{ (2 + e^{-2\tau_d/\tau_c}) \delta(\Omega) + \frac{\tau_c [1 - e^{-2\tau_d/\tau_c} (\cos \Omega \tau_d + \frac{2}{\Omega \tau_c} \sin \Omega \tau_d)]}{2\pi (1 + \frac{1}{4} \Omega^2 \tau_c^2)} \right\} \tag{B.4}$$

For the delay time is much longer than the coherence time, Equation B.4 leads to the well-known result that the spectral density is given by

$$W_I(\Omega) = s_d^2 I_0^2 \left[2\delta(\Omega) + \frac{\tau_c/2\pi}{1 + \frac{1}{4} \Omega^2 \tau_c^2} \right] \tag{B.5}$$

which has a linewidth twice of that of the laser. This property is widely used to experimentally determine the laser's linewidth.